

Journal Pre-proof

Modelling the effects of patch-plug configuration on the impact performance of patch-repaired composite laminates

Haibao Liu, Jun Liu, Zoe E.C. Hall, Richard A. Brooks, James W.M. Crocker, Adam M. Joesbury, Lee T. Harper, Bamber R.K. Blackman, Anthony J. Kinloch, John P. Dear

PII: S0266-3538(23)00010-6

DOI: <https://doi.org/10.1016/j.compscitech.2023.109917>

Reference: CSTE 109917

To appear in: *Composites Science and Technology*

Received Date: 12 October 2022

Revised Date: 20 December 2022

Accepted Date: 7 January 2023

Please cite this article as: Liu H, Liu J, Hall ZEC, Brooks RA, Crocker JWM, Joesbury AM, Harper LT, Blackman BRK, Kinloch AJ, Dear JP, Modelling the effects of patch-plug configuration on the impact performance of patch-repaired composite laminates, *Composites Science and Technology* (2023), doi: <https://doi.org/10.1016/j.compscitech.2023.109917>.

This is a PDF file of an article that has undergone enhancements after acceptance, such as the addition of a cover page and metadata, and formatting for readability, but it is not yet the definitive version of record. This version will undergo additional copyediting, typesetting and review before it is published in its final form, but we are providing this version to give early visibility of the article. Please note that, during the production process, errors may be discovered which could affect the content, and all legal disclaimers that apply to the journal pertain.

© 2023 Published by Elsevier Ltd.



Author statement:

Haibao Liu: Methodology, Formal analysis, Writing- Original draft preparation.

Jun Liu: Investigation, Data curation.

Zoe E. Hall: Investigation.

Richard A. Brooks: Investigation, Data curation.

James W.M. Crocker: Investigation.

Adam M. Joesbur: Investigation.

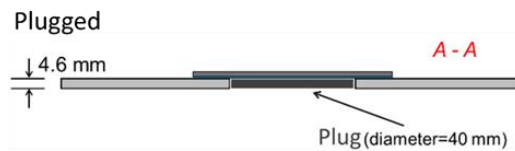
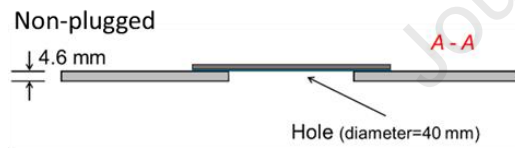
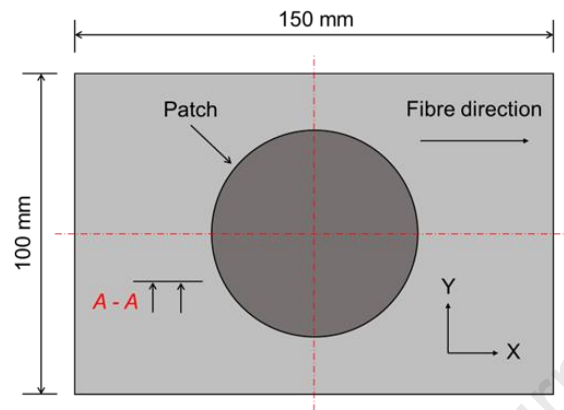
Lee T. Harper: Writing-Reviewing and Editing.

Bamber R.K. Blackman: Writing- Reviewing and Editing.

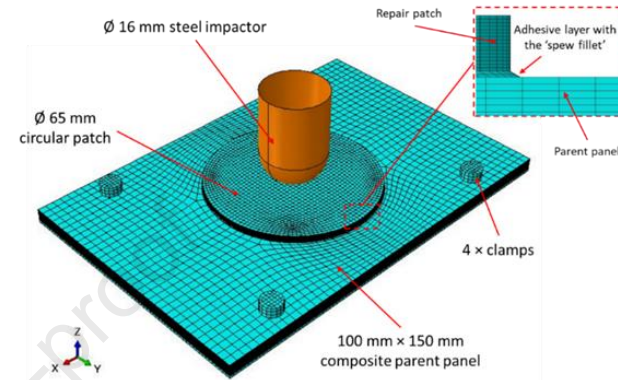
Anthony J. Kinloch: Methodology, Writing- Reviewing and Editing.

John P. Dear: Writing- Reviewing and Editing, Supervision, Funding acquisition.

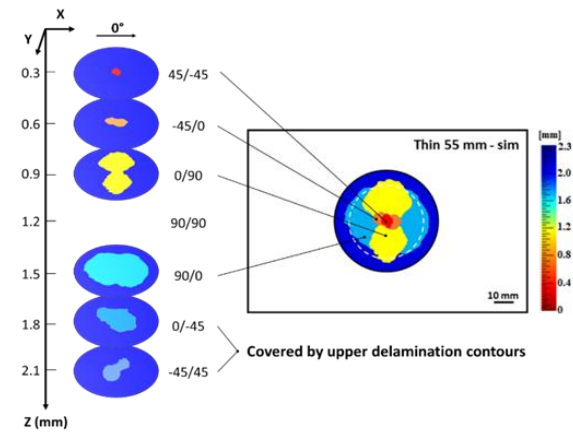
Repair configuration



Model development



Numerical prediction



Modelling the effects of patch-plug configuration on the impact performance of patch-repaired composite laminates

Haibao Liu^{1,*}, Jun Liu¹, Zoe E.C. Hall¹, Richard A. Brooks¹, James W.M. Crocker¹, Adam M. Joesbury², Lee T. Harper², Bamber R.K. Blackman¹, Anthony J. Kinloch¹, John P. Dear^{1,*}

¹*Department of Mechanical Engineering, Imperial College London, South Kensington Campus, London, SW7 2AZ, UK*

²*Composites Research Group, University of Nottingham, University Park, Nottingham, NG7 2RD, UK*

*Correspondence to: Dr Haibao Liu (haibao.liu@imperial.ac.uk) and Prof John P Dear (j.dear@imperial.ac.uk)

Abstract

The patch-plug configuration has been widely used to repair composite structures and restore the structural integrity of damaged composites. In the present research, single-sided CFRP patch-repaired panels, with different patch-plug configurations, are prepared. This is where a circular-shaped damaged area has been removed and a CFRP patch has been adhesively-bonded onto the panel. In some cases, a CFRP plug is inserted into the hole, caused by removal of the damaged area, before the patch is applied. Such patch-repaired panels, and the pristine CFRP panel, are subjected to a low-velocity impact at an energy of 7.5 J. These impacted pristine and repaired panels are then examined using ultrasonic C-scan and optical microscopy to inspect the impact-associated permanent indentation, interlaminar and intralaminar damage. A finite element analysis (FEA) model, which significantly extends a previously validated elastic-plastic (E-P) numerical damage model, has been developed to predict the impact behaviour of the pristine CFRP panel and the various designs of patch-repaired CFRP panels. The comparison between the experimental and numerical results for all the studied cases shows the maximum deviations for the loading response and the damage area are 12 % and 15 %, respectively. The good agreement between the experimentally-measured impact properties and those predicted using the numerical model demonstrates that the model is a useful design tool.

Keywords:

Composite laminates; Patch repair; Impact behaviour; Damage mechanisms; Numerical modelling.

Composite materials based upon carbon-fibre reinforced-plastics (CFRPs) have been increasingly employed in aircraft structures over recent years. However, such materials may suffer a significant loss of performance when subjected to an impact loading [1-13]. Of particular concern is that an impact may lead to damage, such as intralaminar and interlaminar, i.e. delamination, damage, which then reduces the cyclic-fatigue properties of the composite component or structure. Thus, the initial impact performance of the pristine CFRP is of interest because there are many ways that an impact may arise. For example, from an impact via dropped tools, bird strikes, hail stones, runway debris, airport equipment striking the fuselage and hard landings. These impact events may lead to damage, which will require repairs to be undertaken to recover the mechanical performance of the composite material. Naturally, the impact performance of the repaired CFRP is also of interest.

There are two main types of repair techniques for composite materials, namely patch and scarf repairs. Both the patch and scarf repairs have been extensively employed in industrial practice. Airbus and Boeing both have well defined protocols for composite repairs. EDF also have procedures for wind turbine blades, which can be found in [14]. Generally, patch repairs are recommended for secondary structural components, as they are more straightforward and sufficiently effective. Scarf repairs are often preferred for composite structures requiring aerodynamic performance. Scarf repairs give lower stress concentration and better aerodynamic efficiency. To evaluate the effectiveness of repair techniques, tensile, compressive, flexural and impact testing can be employed to characterise the recovered stiffness and strength [15-18]. In the case of secondary and non-critical structure repair, the adhesively-bonded patch repair has been widely used, in which the material is typically bonded to the parent composites as a patch via the use of adhesive-bonding techniques. There have been many papers which have considered the adhesively-bonded patch repair of damaged CFRP panels [15-24]. For example, Soutis et al. [19, 20] have shown that using a relatively simple patch consisting of an adhesively-bonded external patch bonded to a CFRP panel, to repair a hole in the panel, led to a recovery of nearly 80% of the initial compressive strength. They also found that the thickness of the patch influenced the effectiveness of the patch repair. Tie et al. [23, 24] have studied the impact behaviour of single-sided, CFRP patch repairs which had been adhesively-bonded to a CFRP parent panel. Using an impact velocity of $3.25 \text{ m}\cdot\text{s}^{-1}$ and an impact energy of 13.2 J, they examined various designs of patches and reported that the shape of the patch also influenced the effectiveness of the patch repair. The design of the patches included circular, square, hexagonal and octagonal shaped patches, which all had the same nominal area. They found that the use of the circular-shaped patch gave the best recovery percentage for the patch-repaired CFRP panel.

Now, several researchers [25-29], have recently modelled the impact damage in composites and derived the relationships between the different types of observable damage and the permanent indentation and matrix cracking that have been shown to be a precursor to delamination. However, these models were not always able to capture the unstable delamination growth and sudden drop in load at the delamination threshold, and were not applied to repaired CFRP composites. With these limitations in mind, a previously proposed computational finite-element analysis (FEA) model [30] is employed in the present research. This novel model incorporates elastic-plastic (E-P) behaviour,

through a power-law relation, to predict the permanent indentation damage and also captures the transverse through-thickness intralaminar matrix cracking, as well as interlaminar, i.e. delamination, damage. Compared to commercially-available three-dimensional (3-D) FEA damage models, which do not incorporate accurate non-linear models, this E-P 3-D FEA composite model is found to be very useful for studying the impact of composite repair geometries, which exhibit relatively complex mechanical behaviour and damage modes.

In the present work, single-sided CFRP patch repairs, which are adhesively-bonded to the damaged CFRP parent panel, are subjected to a low-velocity impact at an energy of 7.5 J. For the repair panels, a hole, which represents the removal of the impact damage, is cut-out from the centre of a pristine panel to create the parent panel. A single-sided, circular CFRP patch is then bonded to the parent panel over the hole generated. Furthermore, in some designs, a CFRP plug is used to fill the hole generated in the parent panel. The effects of the design of the patch, for example its diameter and thickness and the presence, or not, of a plug, are studied. The E-P 3-D FEA model detailed in [30] has been employed to predict the impact behaviour of the pristine panel and the various designs of patch-repaired CFRP panels. For the composite repair designs, this FEA model has had to be significantly extended to include an adhesive layer, which bonds the patch to the parent panel, and to include the plug for the plugged repairs. The novel aspect of the present research is that, for the first time, the effects of the design of the patch and plug on the impact behaviour of repaired composite panels are thoroughly studied using a combined experimental and numerical methodology. Detailed experimental measurements and numerical predictions, including the load response, the permanent indentation caused by the impactor and impact-associated damage, e.g. matrix cracking and delamination, are presented for the repaired CFRP composites using the various patch-repair designs.

2. Experimental studies

2.1. Materials and panels

The CFRP flat panels had a quasi-isotropic lay-up of $[45_2/-45_2/0_2/90_2]_s$ and were made using a unidirectional carbon-fibre, epoxy-matrix prepreg ('MTC510-UD300-HS-33%RW', SHD Composite Materials Ltd, UK). An autoclave was employed and the panels were cured at 110°C for 120 minutes. The glass transition temperature of the cured epoxy matrix was 133°C. In the CFRP panels the 0° plies were aligned with the longer edge of the panels and the panel had a nominal thickness of 4.6 mm, see Fig. 1. The rectangular panels were 150 mm x 100 mm in size.

The patch-repaired CFRP panels were manufactured by removing a 40 mm diameter disk from the centre of a pristine CFRP panel to represent the impact-damaged area of a pristine CFRP panel, which now became the 'damaged', parent, CFRP panel. The repair patch was a disc of CFRP which was either 55 mm or 65 mm in diameter. In addition, two different thicknesses of patch were used: the thinner patch had a nominal thickness of 2.3 mm, with a lay-up of $[45/-45/0/90]_s$ whilst the thicker patch had a thickness of 4.6 mm with the same lay-up, i.e. $[45_2/-45_2/0_2/90_2]_s$, as that of the parent CFRP. (Note: when the patch repair approach is employed to repair the aerodynamic surface, thinner patches are often considered to be more appropriate than thicker patches and where possible the patch should have minimal protrusion and ideally be scarfed into the surface, so as not to adversely affect the aerodynamic

benzene), the size tolerances for the hole that was cut out from the pristine panel and for the patch was ± 0.1 mm. The patch repair was positioned with a fibre-orientation in the same direction as that of the parent panel and was then bonded to the parent CFRP using a single-layer of a toughened epoxy-film adhesive ('MTFA-500', SHD Composite Materials Ltd, UK). The film adhesive had a nominal thickness of 0.25 mm. The surfaces of the parent and the patch were prepared prior to bonding using 50 grit sanding-discs and were then cleaned with acetone. In some cases, the patch-repaired panels were made using a push-fit plug of the CFRP parent composite to fill the 40 mm hole, which was again orientated in the same direction as the parent panel. For other designs of patch repairs the hole was left unfilled, i.e. non-plugged. The adhesive layer was cured at 130°C for 90 minutes to complete the manufacture of the patch-repaired panels.

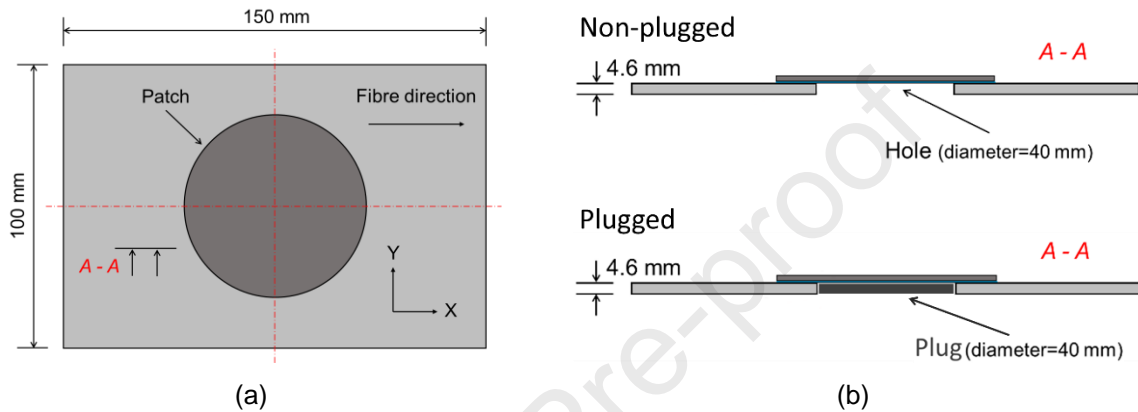


Fig. 1. Schematics of the patch-repaired CFRP panels: (a) the top view where the diameter of the patch was either 55 mm or 65 mm, with a thickness of 2.3 mm or 4.6 mm, and (b) the side cross-section view of the non-plugged and plugged patch-repaired CFRP panels. (Note that in some cases the patch-repaired panels were made using a push-fit plug of the CFRP parent composite to fill the 40 mm diameter hole.)

2.2. Compressive strength testing

To assess the compressive strength of patch-repaired composite laminates, compressive strength testing has been conducted on both pristine and patch-repaired composite panels as shown in Fig. 2. This is with the composite panels being supported by the testing rig, which was originally designed for the compression-after-impact experiments. Such a testing rig inhibits global buckling behaviour through effective support of the edges of composite panels. Speckle strain mapping was also employed to make sure the applied load was uniform along the top edge of the specimen. Displacement control was adopted in this compressive strength testing, with an applied loading rate of 0.5 mm/min to minimise dynamic effects. Experimental data were directly recorded on a PC and the accompanying software (Instron, USA) gave both the reaction load and resulting displacement of the composite panels for this compression event. Three composite specimens were tested for each case.

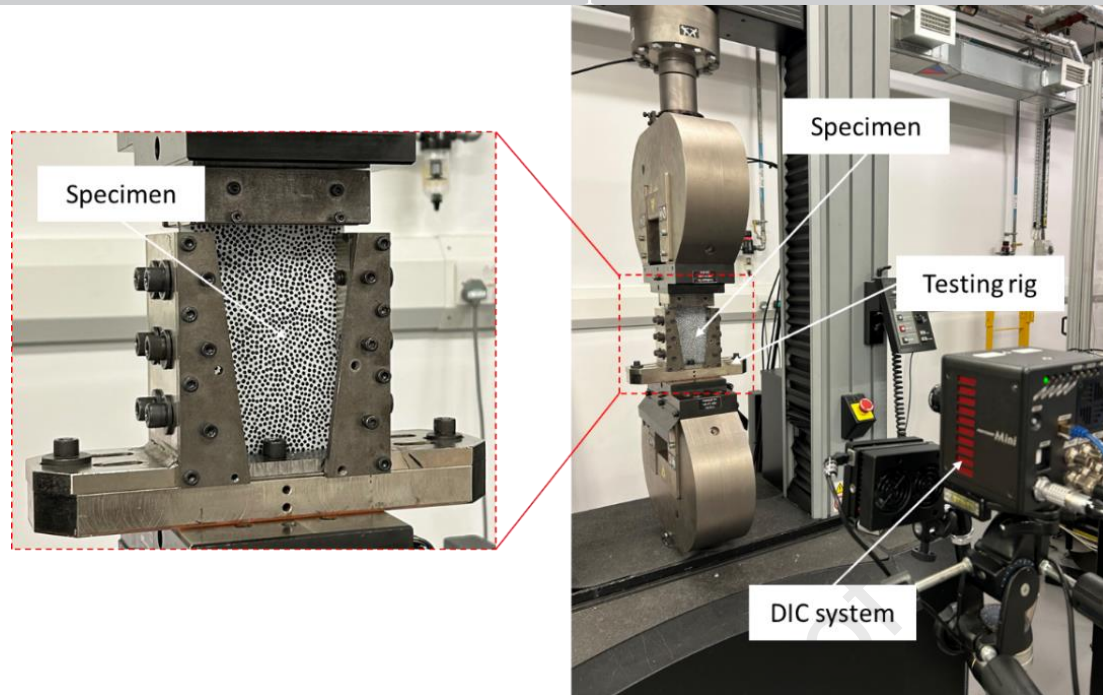


Fig. 2. Experimental set-up for compressive strength testing.

2.3. *Drop-weight impact testing*

The drop-weight impact testing scheme described in ASTM 7136 [31] was employed to investigate the impact behaviour of the pristine and patch-repaired panels, as shown schematically in Fig. 3. In these experiments, the pristine and the patch-repaired panels were clamped in place on a steel picture-frame platform, which had a 125 mm x 75 mm cut-out window. A hemispherical steel impactor, with a diameter of 16mm and a mass of 5.26 kg, was used to strike the pristine and the patch-repaired panels with an impact energy level of 7.5 J. The impact force was instantaneously measured by a dynamic load-sensor located in the impactor. A catching system was used to prevent further impact events from occurring after the initial impact and no software filtering was applied to the load versus time data. These data were directly recorded on a PC and the accompanying software (CEAST, Italy) gave both the impact load and resulting displacement of the composite panels as a function of time for the impact event. Two duplicate specimens were tested for each panel design.

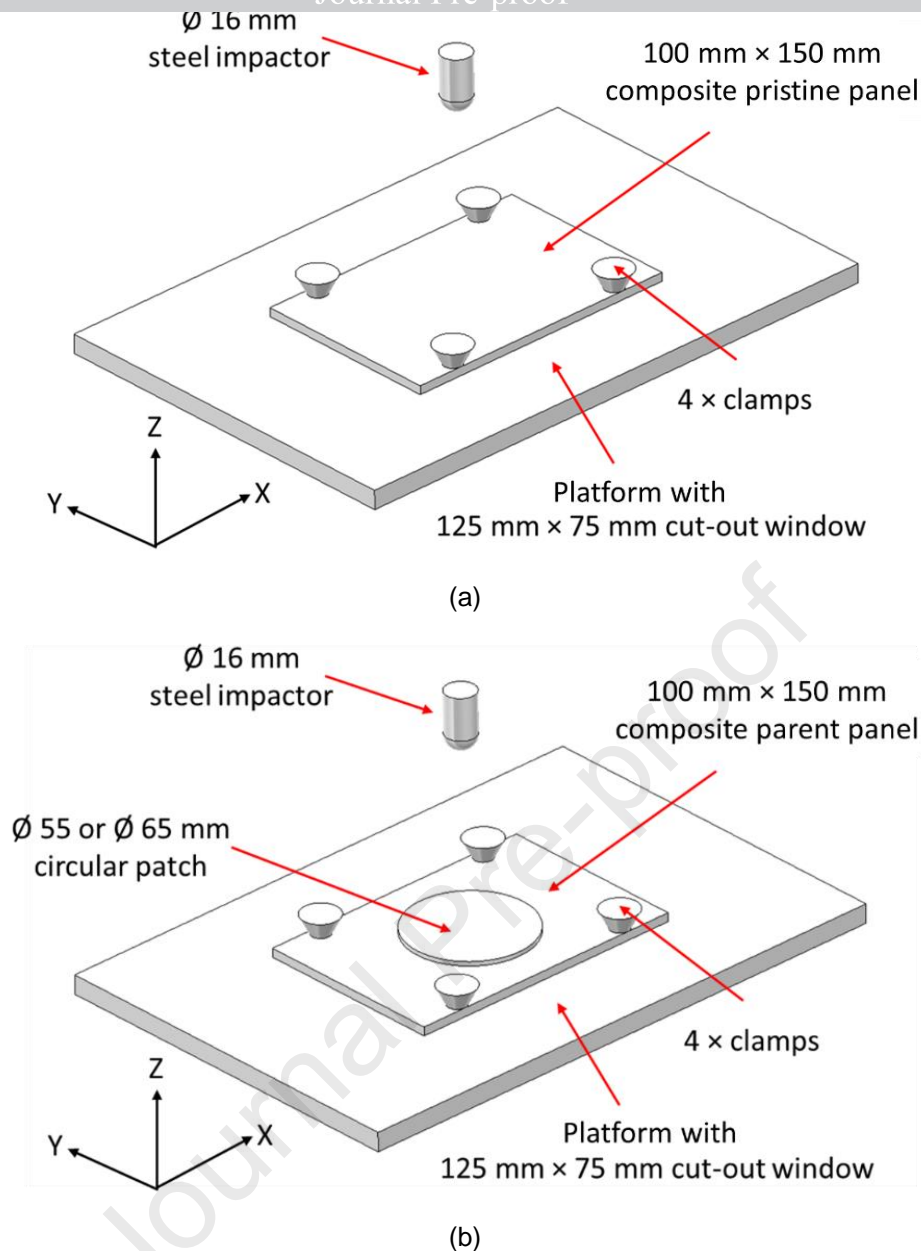


Fig. 3. Schematic of the drop-weight impact testing set-up for (a) the pristine panel and (b) the patch-repaired panel.

2.4. C-Scan and optical microscopy inspections

All the post-impacted pristine and the patch repaired composite specimens were examined using a portable C-scan device ('Prisma 16:64 TOFD', Sonatest Ltd, UK) which was fitted with a 5 MHz probe. The results were presented as the time-of-flight C-scan maps, which showed the extent of any delaminations as a function of the depth through the thickness of the panel. The areas of the delamination footprints were then calculated. An optical microscope was also employed to inspect the damage in the pristine and the patch-repaired panels, whereby post-impacted panels were first sectioned using a diamond saw to obtain the initial cross-sections, which were then polished in water using silicon carbide grinding papers, using a series of grades from P180 to P4000, and then finely polished using a polishing cloth with a diamond suspension fluid.

3.1. Overview

A finite-element analysis (FEA) numerical model, integrating an elastic-plastic (E-P) user-defined sub-routine [30] and cohesive surface models, has been employed to predict the impact behaviour of composite repairs with different patch and plug designs. The FEA model was implemented in 'Abaqus 2020' (Dassault Systemes, France) and the overall flowchart is shown in Fig. 4. (Note that the basic model in [30] was implemented in 'Abaqus 2018' but the later version of 'Abaqus 2020' was used in the present research. A check confirmed that no differences in the results were recorded using these two versions of 'Abaqus'.) All the methodologies and equations that are used in the numerical model, as given in this figure, are derived and presented in [30] where the equations are numbered as in Fig. 4. In [30] the reader can follow the logical development of this numerical model, including the novel E-P model that has been developed, the failure criteria used and how crack initiation and propagation for the intralaminar and interlaminar damage regions are defined and quantitatively modelled. In the present extended FEA model an adhesive layer has been added between the patch and the parent panel, which can deform and transmit stress across the interface, and the presence of a CFRP plug has been included when appropriate. In the FEA model, the basic mechanical properties of the composite plies and the adhesive layer, including strength, modulus, Poisson's ratio and fracture toughness, etc., that are required for the simulation were obtained from the manufacturer's data sheets and from the literature [30, 32-37] and are given in Table 1.

The novel E-P in-house user-defined sub-routine which has been embedded into the FEA computational model to capture the E-P material response prior to the damage initiation enables a more accurate prediction of the impact behaviour of the composite panels and allows the modelling of any permanent indentation arising from the impact to be simulated. The constitutive relation for the E-P model was obtained by combining the classical elastic model with a plastic model. To address the complex stress state, the effective stress and effective strain were defined in the extended E-P model and the relationship between them was defined via a power-law function. The interlaminar damage involves the initiation and growth of delaminations between the plies that make up the composite laminate and was captured using the 'Abaqus' built-in surface-based cohesive surface solution, in which the traction is a function of the displacement using a bilinear cohesive law for a linear-softening material model. The energy under the bilinear cohesive law was equivalent to the interlaminar fracture energy, G_c . Before the initiation of any delamination, the cohesive law possessed linear-elastic behaviour with a stiffness of k_t . Once the interlaminar damage criterion was satisfied the cohesive stiffness was degraded linearly until separation of the interface occurred, i.e. interlaminar cracking occurred, when the traction tended to zero and the maximum failure displacement was now attained. It should be noted that the initiation and growth of any intralaminar damage significantly influenced the extent of interlaminar damage and hence these two damage modes were modelled to be interactive in the 'Abaqus' simulation. In the intralaminar damage model, the 3-D damage criteria derived by Daniel et al. [30, 38-40] were employed to capture the onset of the initiation of intralaminar damage such as matrix cracking, etc. These criteria are partially interactive, which means that more than one stress component was employed and different types of intralaminar damage may be introduced into a composite ply via various stresses, including the longitudinal tensile and compressive stresses, transverse tensile and

compressive stresses, through thickness tensile and compressive stresses, transverse and through thickness shear stresses. Eight corresponding damage variables were defined [30] to indicate the propagation of intralaminar damage in a composite ply. These damage parameters have the value of 0 when the element is undamaged and 1 when fully damaged and they were used to degrade the elasticity matrix to form the damaged elasticity matrix for describing the behaviour of impact-damaged material. Again, all the relevant details and equations that were used are presented in [30].

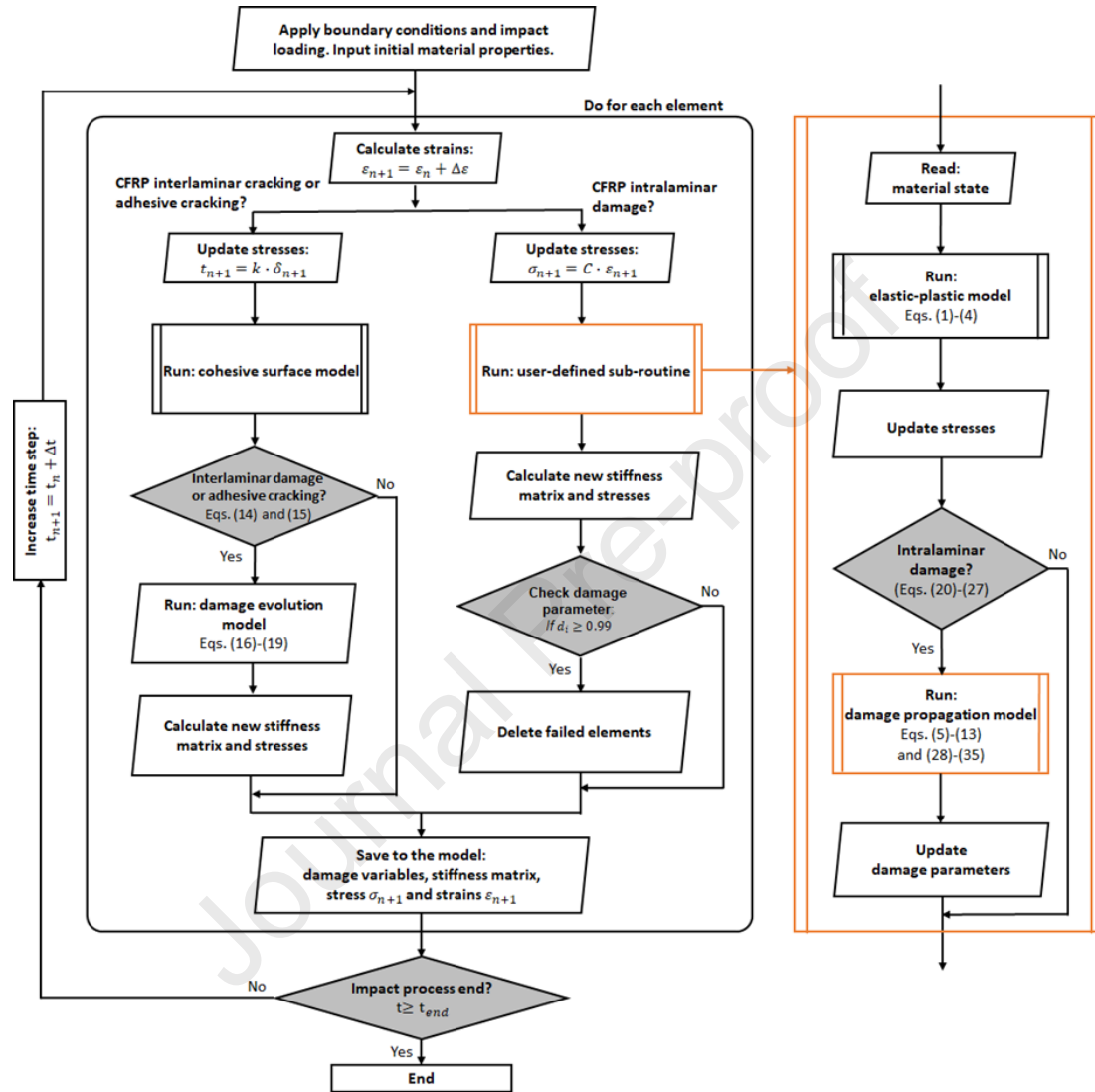


Fig. 4. The implementation of the E-P, 3-D FEA numerical damage model showing schematically the overall flowchart for one computational time-step and a single integration point. Both the flowcharts for the main model and for the elastic-plastic (E-P) user-defined sub-routine are shown. This FEA modelling simulation of the impact event would be run typically over a time-scale, t , of 0 to ca. 8 ms, with ca. 100 time-steps being employed. The simulation runs were stopped when the defined total computation time for the impact simulation event had expired. (All the methodologies and equations that are used in the above FEA model are derived and presented in [30], where they are numbered as above.)

Table 1. The properties, as defined in [30], of the unidirectional CFRP and the rubber toughened adhesive used in the FEA modelling studies [30, 32-37].

Property	CFRP	Adhesive
Moduli (GPa)	$E_{11} = 115; E_{22} = E_{33} = 8.2$ $G_{23} = 3.6; G_{12} = G_{13} = 3.6$	$E = 2.1$
Poisson's ratio	$\nu_{23} = 0.34; \nu_{12} = \nu_{13} = 0.34$	$\nu = 0.3$
Strength, S, values (MPa)	$S_{1t} = 2282; S_{2t} = S_{3t} = 54$ $S_{1c} = 1067; S_{2c} = S_{3c} = 200$ $S_{12} = S_{13} = S_{23} = 99$	$S = 45.0$
Intralaminar ply fracture energies (kJ/m ²)	$G_{Ic ft} = 133; G_{Ic fc} = 40$ $G_{Ic mt} = 0.4; G_{Ic mc} = 1.3; G_{IIc ms} = 1.3$	$G_{Ic} = 2.3; G_{IIc} = 2.8$
Interlaminar ply or adhesive fracture energies (kJ/m ²)	$G_{Ic} = 0.4; G_{IIc} = 1.3$	$G_{Ic} = 2.3; G_{IIc} = 2.8$
Benzeggagh–Kenane exponent	$\eta = 1.45$	$\eta = 1.45$
Cohesive strengths (MPa)	$t_{33}^0 = 43.0; t_{31}^0 = t_{32}^0 = 50.0$	$t_{33}^0 = t_{31}^0 = t_{32}^0 = 45.0$
Initial cohesive law stiffness (MPa/mm)	$k_i = 6.4 \times 10^5$	$k_i = 6.4 \times 10^5$
E-P model: coefficient, a_{66} , and material constants, A and n	$a_{66} = 2.7; A = 3.14 \times 10^{-13} \text{ MPa}^{-n};$ $n = 4.19$	N/A

3.2. The finite-element analysis (FEA) model

To simulate the impact events on the pristine and the patch-repaired composite panels, FEA models were run on the 'Abaqus 2020' platform. Created models for the pristine and patch-repaired panels are shown in Fig. 5. For the pristine panel, composite plies with a 100 mm × 150 mm dimension were modelled as three-dimensional (3-D) deformable parts and stacked together based on the lay-up of [45₂/-45₂/0₂/90₂]_s, to form the 4.6 mm thick pristine composite panel. The pristine panel was meshed using eight-noded linear-reduced integration (C3D8R) solid elements with a size of 1.5 mm × 1.5 mm. For the patch-repaired panel without a plug, a parent panel with a 40 mm diameter hole and a repair patch with various diameters (i.e. 55 mm or 65 mm) and thicknesses (i.e. 2.3 or 4.6 mm) were modelled as 3-D deformable parts. The parent panel and the 4.6 mm thick patch had the same lay-up as the pristine panel of [45₂/-45₂/0₂/90₂]_s, and the 2.3 mm thick patch had a lay-up of [45/-45/0/90]_s. Both the parent panel and the patch were meshed using C3D8R solid elements where 3 mm × 3 mm elements were employed for the parent panel and 1.5 mm × 1.5 mm elements were employed for the patch. The adhesive layer in the patch-repaired specimen was modelled using 1.5 mm × 1.5 mm C3D8R elements and an exuded spew fillet of adhesive was modelled at the edge, as shown in Fig. 5. Cohesive surfaces were employed to model the contacts between the composite plies with different fibre directions to capture the interlaminar failure as well as the adhesive film/patch and the adhesive film/panel contacts to capture adhesive bonding failure if it should occur. The general contact algorithm was used to govern the global contact. The composite damage model described above was also employed to simulate the impact of the patch-repaired panels with a plug, where the plug had the same thickness and lay-up as

the parent panel and the plug/adhesive interface, as for the patch/adhesive film interface, was again employed. It was assumed that no relative movement occurred between the parent panel and the pushed-in plug, so a tie-contact mode was implemented in 'Abaqus' to define this contact. The hemispherical steel impactor and the steel picture-frame platform were modelled as an analytical rigid surface and a discrete rigid body, respectively. Friction coefficients were defined as 0.25 and 0.2 for the composite/composite interfaces and the composite/steel interfaces, respectively. In the simulation, composite panels were located on a 100 mm × 150 mm rigid platform with a 75 mm × 125 mm cut-out window. The rigid impactor was given an initial velocity to strike the composite laminates. Four clamps were employed to constrain the vertical movement and also provide the friction which can inhibit the in-plane slip of composite laminates during impact. The simulations of the impact on the pristine and patch-repaired composite panels were undertaken using 16 CPUs on a Linux Cluster with a run time of 25 and 32 hours, respectively.

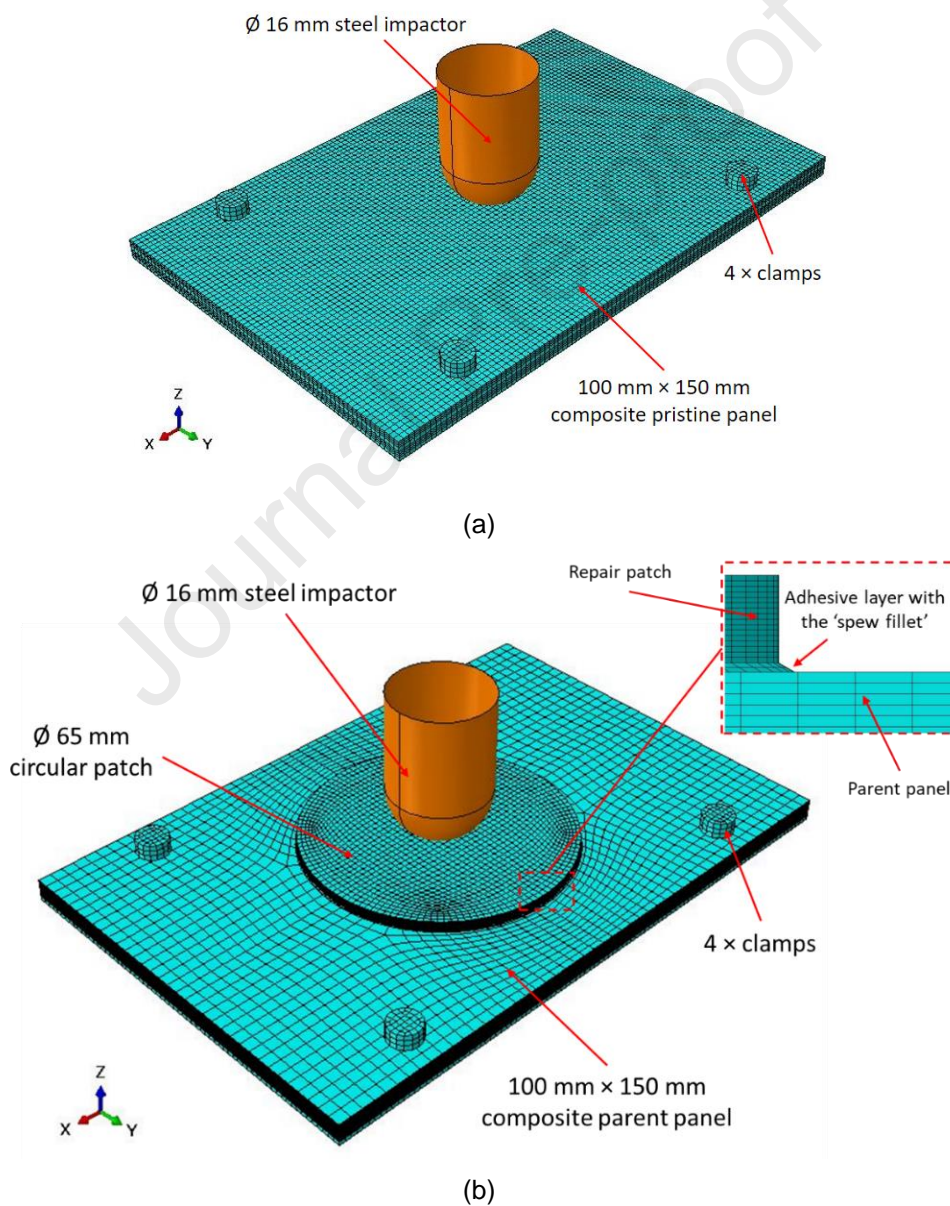


Fig. 5. Finite-element analysis (FEA) model for simulating the impact event on: (a) a pristine CFRP panel and (b) a patch-repaired CFRP panel (shown with a 65 mm diameter patch).

4.1. Compressive strength

The load-carrying capability of the non-plugged patch-repaired CFRP panels was characterised through the quasi-static in-plane compression tests. The compressive loading response measured from these non-plugged patch-repaired CFRP panels have been presented and compared with the loading response of pristine panels in Fig. 6. To be noted is that the stiffness of the patch-repaired panel is comparable with the pristine panel. The average maximum compressive load achieved by the pristine and the 55 mm thin patch repaired panels are 136.5 kN and 84.7 kN respectively, which give average compressive strengths of 297 MPa and 184 MPa respectively. The comparison between the average compressive strengths obtained the pristine and the 55 mm thin patch-repaired panels shows that about 62% of the original compressive strength has been restored by using this patch repair approach, which demonstrates reasonable effectiveness for the patch repair. This is with the benefit of removing delamination, if it were to occur from impact, before a patch (and/or a plug) is attached. Similar samples are employed below for the impact studies.

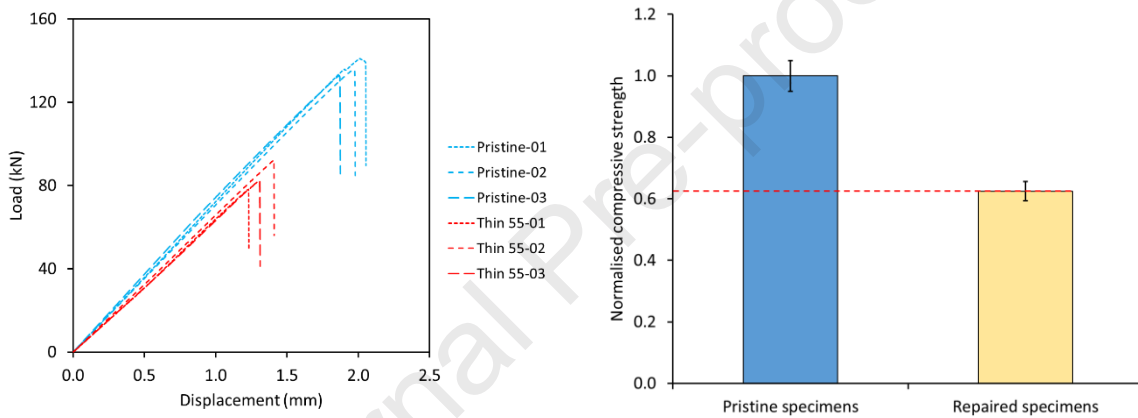


Fig. 6. Experimental results obtained from compressive strength testing performed on the pristine and 55 mm thin patch-repaired composite panels: (a) the loading history and (b) the normalised compressive strengths.

4.2. Experimental results for impact loading responses and overall interlaminar damage

The loading responses for the pristine panels and the different designs of non-plugged patch-repaired CFRP panels were measured from the drop-weight impact tests and are compared in Fig. 7. Several interesting observations may be made. Firstly, the results from the duplicate tests for a given type of test panel are in excellent agreement which indicates very good repeatability of the experimental test data. Secondly, in all cases there are relatively small amplitude, sinusoidal oscillations on the rising part of the load versus time, and the load versus displacement, experimental curves which are especially pronounced for the pristine CFRP panel. Such oscillations have previously been discussed in detail [30, 41-47] and are indicative of mass-spring oscillations. Thirdly, the patch-repaired panels using relatively thin repair patches, i.e. with a thickness of 2.3 mm, gave an impact response with a lower maximum load and reduced stiffness, as seen in the load versus displacement curves, when compared to that of the pristine panel. Fourthly, increasing the diameter of the patch, for a given patch thickness of 2.3 mm, only changes the impact response very slightly, as shown in Fig. 7, where, for example, the difference between the maximum loads obtained the 55 mm and 65 mm diameter (thin) patch-repaired panels is

less than 0.1. This result is supported from the C-scan shown in Fig. 6, where providing the patch diameter is appreciably larger than the hole, then the delamination, i.e. interlaminar, damage tends to be almost completely confined to the patch directly above the hole. Finally, to assess the effect of having a thicker patch, which had the same thickness as that of the parent CFRP, a patch of 4.6 mm thickness with the larger diameter of 65 mm was evaluated. It is evident for a panel with a 65 mm diameter patch of thickness 4.6 mm, the bending stiffness was slightly more than for the pristine panel, see the load versus displacement curves in Fig. 7b. The area where the patch overlaps with the parent material gives an annulus or ring of overlapping composite laminate of thickness 9.2 mm, which includes both patch and parent panel. It is this 9.2 mm thick overlap area which leads to a significantly higher bending stiffness for the 65 mm thick patch repaired composite panel, compared to the pristine panel. The stiffness for the studied panels follows the sequence from high to low: 65 mm thick patch > pristine > 65 mm thin patch > 55 mm thin patch, which is as to be expected. The stiffness of the panel is one of main factors that can considerably influence the critical load in the loading response curves, which is mainly associated with the localised deformation due to matrix compressive damage and subsequent delamination near the contact zone. For the thick composite panels, the localised deformation in the contact zone tends to be more constrained due to the panel with thicker patch having higher bending stiffness. As a result, higher loads are required to cause localised deformation, which can give a more substantial load drop in the loading response curves. For this reason, the critical load drop and the magnitude of the loads drop follow the sequence from high to low: 65 mm thick patch > pristine > 65 mm thin patch > 55 mm thin patch.

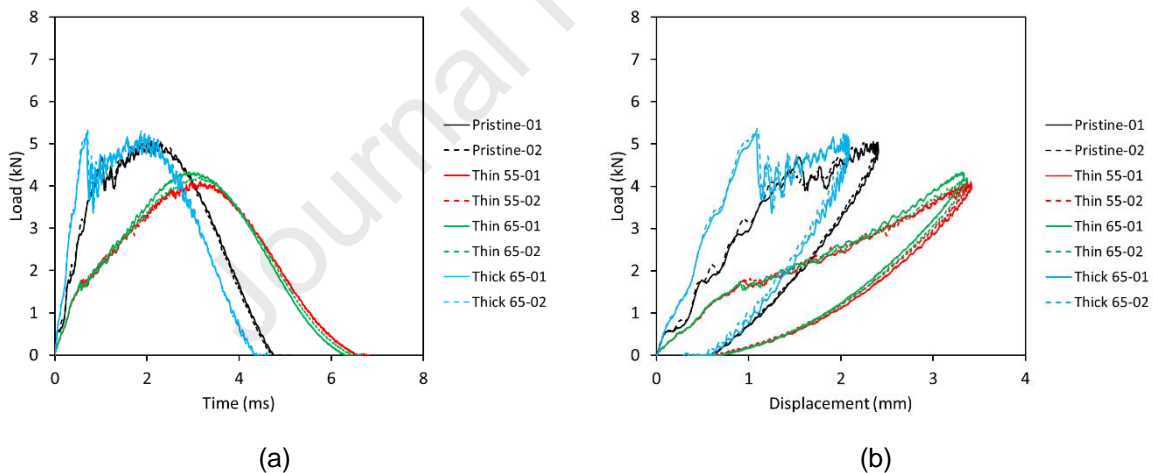
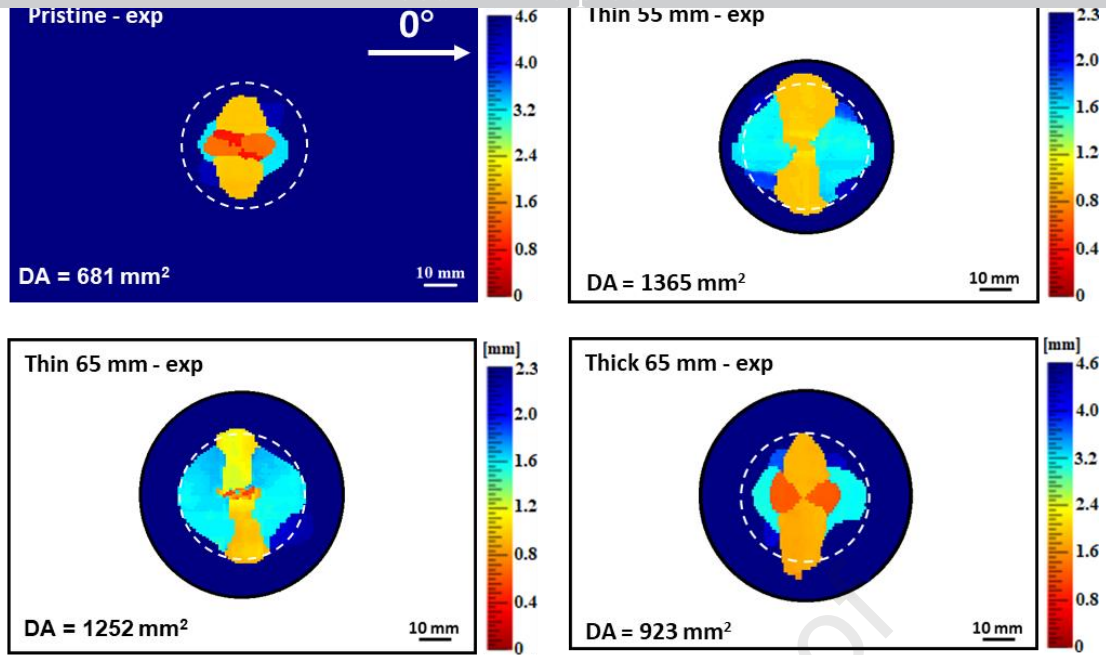


Fig. 7. Loading responses for the pristine and non-plugged patch-repaired composite panels: (a) the load versus time curves and (b) the load versus displacement curves. (Notation: for example, ‘Thin 55’ refers to the thin (i.e. 2.3 mm thickness) 55 mm diameter repair patch, whilst ‘Thick 65’ refers to the thick (i.e. 4.6 mm thickness) 65 mm diameter patch; and ‘01’ and ‘02’ refer to duplicate Tests 1 and 2.)

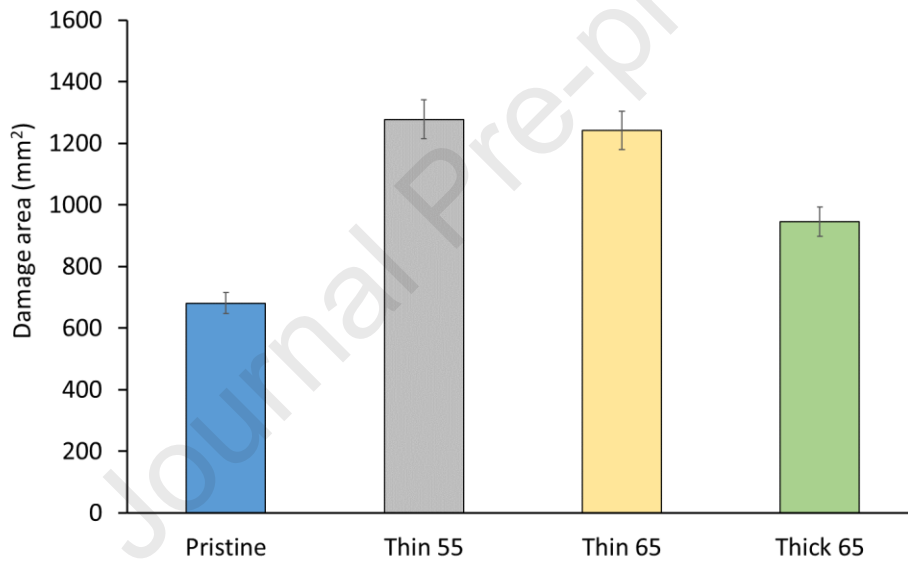
Typical C-scan maps and average damage areas obtained from the pristine and patch-repaired composite panels are presented in Fig. 8 for a range of patch designs. Naturally, there was no hole cut-out from the pristine panel but a white-dashed line is included here to indicate that the damage from the impact was all contained within a 40 mm diameter, justifying the dimensions of the removed area for the patch-repaired panels. For the patch-repaired panels, the white-dashed line represents the 40 mm

diameter hole that was cut out in the interlaminar damage maps, such as Fig. 6a, the right-hand side scale in these figures indicates the location of the delaminations as a function of the depth through the thickness of the panel, where the dark-red colour represents the front (impacted) face and the dark-blue colour represents the rear (non-impacted) face of the composite panel. The 0° fibre direction is also indicated. The areal footprint of the damage, i.e. the damage area (labelled 'DA'), is given at the bottom left in each case and this was determined by counting the number of pixels which had a colour that was not dark blue, since the rear surface simply reflects the ultrasound and appears as being dark blue in colour. These damage areas arise from interlaminar damage, i.e. delaminations, in the panels resulting from the impact event. Delaminations initiate and grow at interfaces where the fibre direction is different in the plies below and above the interface. This is with the delamination propagation dominated by the fibre direction of the ply which is furthest from the impact surface. Localised deformation drives the initiation of matrix cracking and subsequent delamination. Due to the changes in stiffness across the interface between composite plies in different directions, the interfacial shear stresses can drive the crack growth mainly in Mode II (or shear loading) to form a larger delamination area. These delamination processes occur in the pristine specimens as well as the patches of the repaired composite specimens subjected to impact loading.

There are several noteworthy observations. Firstly, the results shown in Fig. 8b reveal that the measured damage areas from the duplicate tests for a given type of panel give a relatively low scatter in the data. Secondly, all the interlaminar damage in the patch-repaired panels is contained within the patch. Indeed, no such damage was ever found in the parent CFRP to which the patch was adhesively-bonded, or within the adhesive layer or at the adhesive/CFRP interfaces either. Thirdly, all the patch-repaired panels possess larger damage areas than the pristine panels. However, a comparison between the C-scan maps obtained from the different designs of repair patches shows that the design can significantly influence the profile and extent of damage due to impact loading. For example, the difference between the average damage areas in the 55 mm and 65 mm diameter thin patch-repaired composite panels is not statistically significant, which reveals that the diameter of the patch has a relatively minor effect on the extent of impact damage. On the other hand, a comparison between the average damage areas obtained for the thin (e.g. DA=1252 mm²) and thick (e.g. DA=923 mm²) 65 mm diameter patches shows that the difference is about 25%, which demonstrates the significant effects that the thickness of the patch has upon the extent of damage. These observations from Fig. 8 agree with the results shown in Fig. 7, where only the use of the 65 mm diameter thick patch (4.6 mm) gave a stiffness and other measured impact parameters, which were comparable to those of the pristine panel. The thinner patch deforms more during an impact, leading to higher levels of delamination. However, as seen in Fig. 8, the extent of the delamination is confined to the region above the hole and, for this reason, the thinner patch is still a reasonably effective repair.



(a)



(b)

Fig. 8. Comparison of C-scan maps and the average damage areas for the pristine and patch-repaired panels after impact: (a) the C-scan maps and (b) the average damage areas calculated from the C-scan maps of the pristine and patch-repaired panels. (The white-dashed line on the pristine panel indicates where the 40 mm hole would be cut-out before any repair was undertaken. For the patch-repaired panels it indicates where the 40 mm diameter hole was cut-out in the parent panel. All the results are from the C-scan experimental ('exp') tests and the error bars in Fig. 8b indicate the scatter measured in the duplicate test panels.)

4.3. Comparison between experimental and numerical results

4.2.1. The overall loading response

Fig. 9 presents the experimental and predicted loading versus time curves obtained from the pristine and patch-repaired composite panels. As may be seen, there is a very good agreement between the

measured experimental results with those predicted using the numerical model. Fig. 9 shows that there is also a very good agreement between the load versus displacement responses obtained from the experiments and from the predictive numerical simulations of the pristine and patch-repaired composites. The experimental impact results for all the composite panels indicate a linear response at the start of loading, followed by a drop in load, or change in gradient, which is associated with damage initiating and propagating. In addition, the magnitude of the maximum loads and displacements, and the displacement at failure, have also been accurately predicted by the numerical model. The level of agreement between the experimental and numerical loading responses demonstrates that the present computational model is capable of accurately predicting the impact behaviour of both the pristine and repaired composite panels. In particular, load drops and changes of stiffness which are indicative of the onset of damage are captured in the modelling.

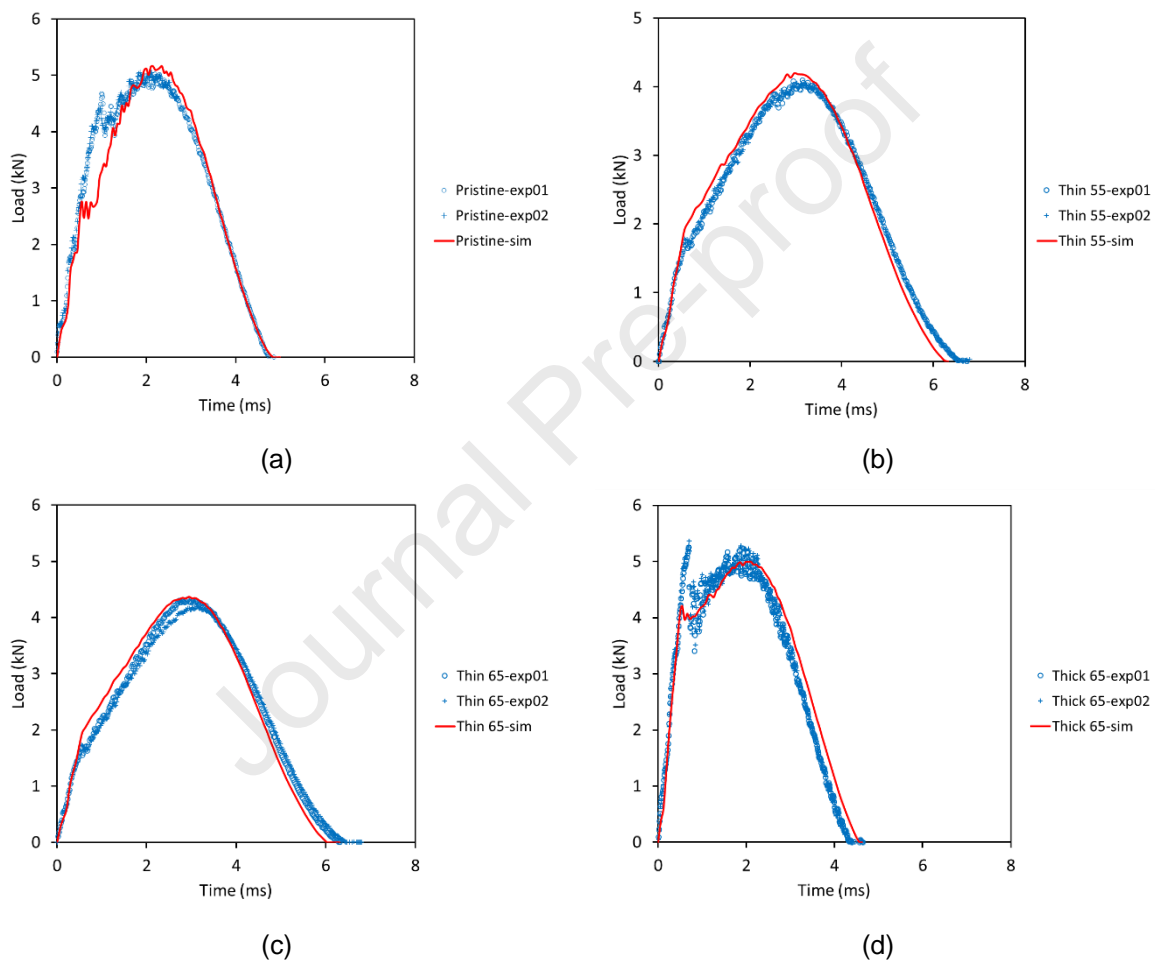


Fig. 9. Experimental results and numerical predictions for the load versus time curves of the pristine and patch-repaired panels with different patch designs. (Notation: for example, ‘Thin 55’ refers to the thin (i.e. 2.3 mm thickness) 55 mm diameter repair patch, whilst ‘Thick 65’ refers to the thick (i.e. 4.6 mm thickness) 65 mm diameter patch; and ‘exp01’ and ‘exp02’ refer to duplicate Tests 1 and 2. The term ‘sim’ refers to the results from the numerical simulation predictions.)

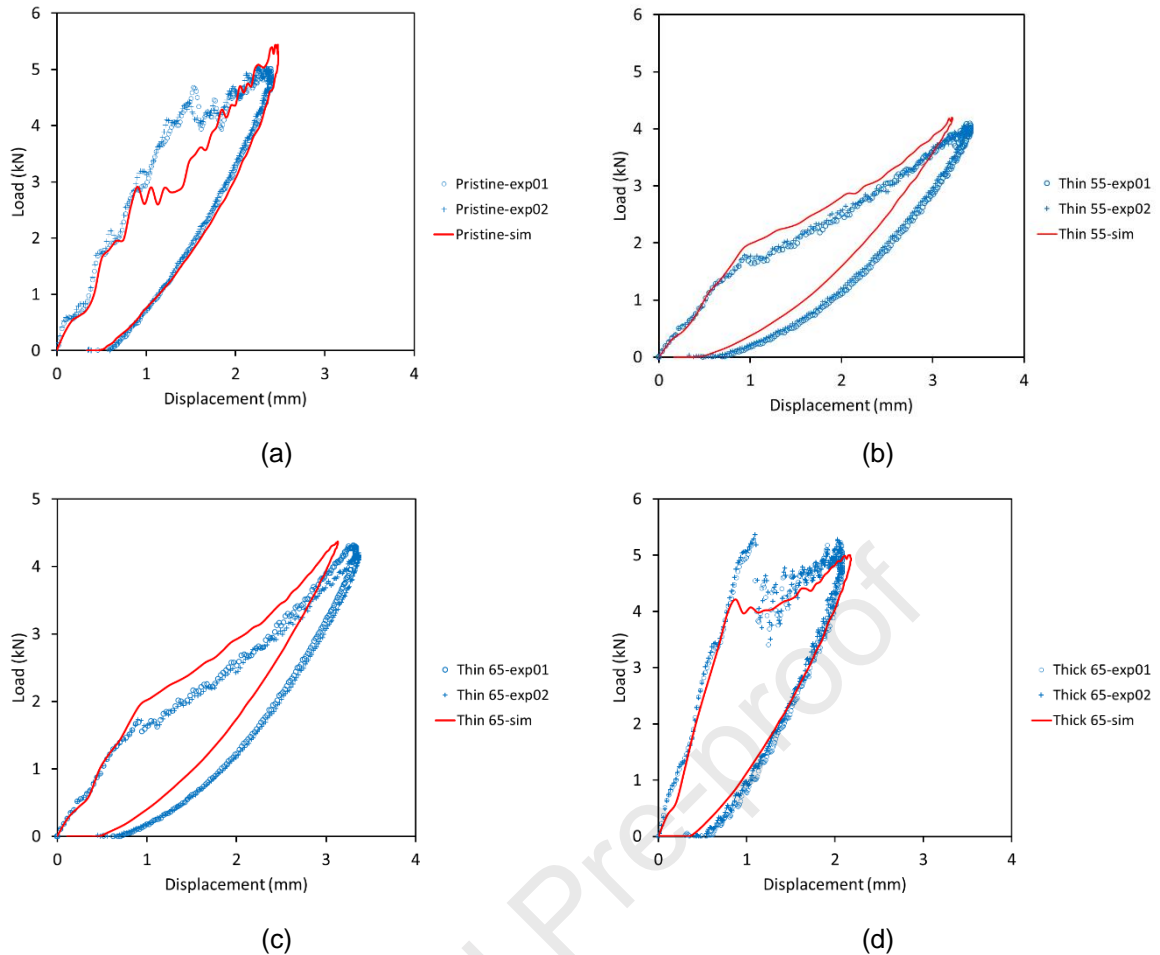


Fig. 10. Experimental results and numerical predictions for the load versus displacement curves of the pristine and patch-repaired panels with different patch designs. (Notation: for example, ‘Thin 55’ refers to the thin (i.e. 2.3 mm thickness) 55 mm diameter repair patch, whilst ‘Thick 65’ refers to the thick (i.e. 4.6 mm thickness) 65 mm diameter patch; and ‘exp01’ and ‘exp02’ refer to duplicate Tests 1 and 2. The term ‘sim’ refers to the results from the numerical simulation predictions.)

4.2.2. Interlaminar damage

Fig. 11 shows the experimental and predicted interlaminar damage footprints obtained from the pristine and patch-repaired composite panels. The first noteworthy point from these results is that the various designs of repair patch give a widespread in the measured values of the interlaminar, i.e. delamination, damage footprint. Such values range from 923 mm² to 1365 mm², with the pristine CFRP panel having suffered 681 mm² of interlaminar damage, see also Table 2. Furthermore, for the patch-repaired panels, all of this interlaminar damage was found to be contained only in the CFRP patch repair material, just above the hole beneath the patch. Secondly, the numerical model predicts the extent of the interlaminar damage relatively accurately, with the largest difference compared to the experimental results being only about 15% for the patch-repaired panel using the 65 mm diameter patch with a thickness of 4.6 mm. As noted above, the colour coding of the delaminations shows their depth through the thickness with a scale bar for the depth on the right of Fig. 11. This scale bar is consistent for both the experimental and predicted damage plots and it can clearly be seen that the delaminations for both the experiments and predictions occur at the ply interfaces, where there is a change of fibre direction, and exhibit a

similar shape and extent through the thickness. This is a powerful feature of the model which is discussed further below.

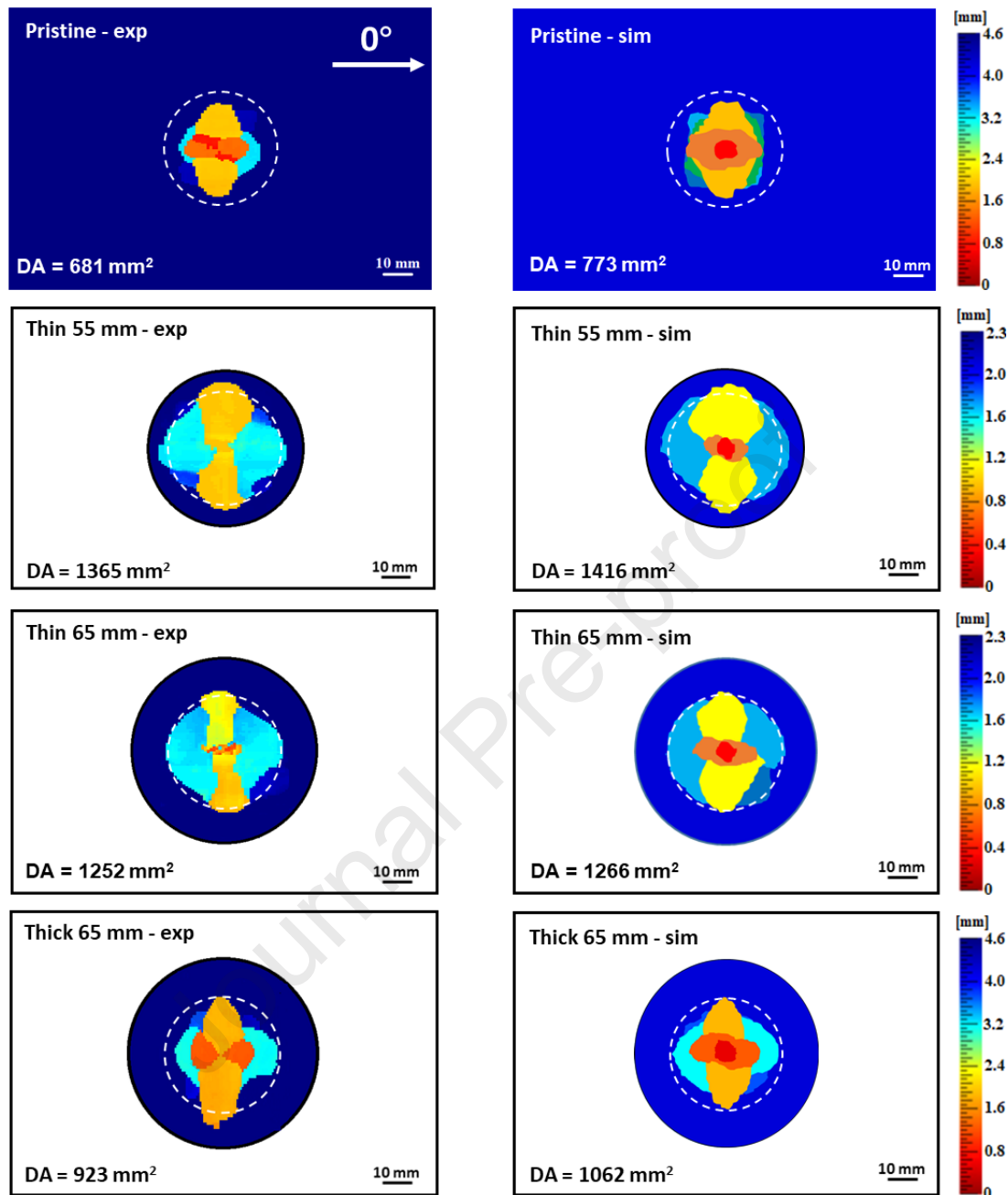


Fig. 11. Experimental (via C-scan) and predicted numerical damage footprints obtained for interlaminar, i.e. delamination, damage for the pristine and patch-repaired panels with different patch designs. (The white-dashed line on the pristine panel indicates where the 40 mm hole would be cut-out before any repair was performed. For the patch-repaired panels it indicates where the 40 mm diameter hole was cut-out in the parent panel.)

Table 21 Comparison between the areas of the damage footprints for interlaminar damage obtained from the experimental studies and the numerical predictions for the pristine and patch-repaired panels using various designs of non-plugged repair patch.

Design of panel:	Pristine	Thin 55 mm	Thin 65 mm	Thick 65 mm
Measured area (mm ²)	681 ± 10%	1365 ± 4.3%	1252 ± 6.7%	923 ± 8.3%
Predicted area (mm ²)	773	1416	1266	1062
Difference in the above	13.5%	3.7%	1.2%	15.1%

To further demonstrate the predictive capability of the numerical damage model, results are shown in Fig. 12 from the numerically predictive simulations of an exploded view for the interlaminar damage at different interfaces in the multi-axial lay-up of the CFRP patch. The patch-repaired panel with a patch of 55 mm diameter and a thickness of 2.3 mm was chosen for this exercise. As may be seen, the extent of the predicted areal numerical damage areas is near a maximum at a depth of 0.9 mm, i.e. at the ply interface just above the central-blocking 90° plies. This peanut-shaped delamination is orientated across the width of the specimen, in the direction of the 90° ply. At the ply interface at a depth of about 1.5 mm, just below the central-blocking 90° plies, the predicted peanut-shaped delamination is large and elliptic in shape and orientated along the length of the panel in the direction of the 0° ply. It should be noted that due to the large delamination on the 90/0 interface, the predicted delaminations below this interface cannot be observed in the overlapped view of the numerical, or experimentally-measured, simple damage footprint maps. Thus, the exploded view in Fig. 12 can be employed to show the details of the delaminations on these interfaces which are obscured by the larger damage footprint areas. These exploded views clearly show that delaminations occur on the interfaces at different depths of the CFRP patch and develop as to be expected from the physics and micromechanics of the impact event demonstrating the capability of the model. For example, the delamination has a characteristic peanut shape with the orientation of the maximum extent of the delamination being aligned in the ply direction beneath the ply interface. The delamination tends to grow in the direction of the ply beneath the ply interface, as this ply can deflect in that direction. Also, delaminations increase in extent as you move away from the impactor face, as they are initiated by localised indentation and associated matrix cracking that occurs under the impactor. The delamination is largest in extent at a depth of about 1.5 mm, as this is just below the neutral axis where the shear stresses reach their maximum. The tendency for a delamination to occur at the 90°/90° interface is low, as the relative bending stiffness of the plies is similar due to the relative fibre orientation of the plies. Finally, there were no indications of any adhesive cracking or adhesive/CFRP interfacial debonding in the patch-repaired specimens at all. These experimental observations are in agreement with the results from the FEA studies, which indeed predicted that no such adhesive cracking or debonding would occur in the impacted patch-repaired specimens. Thus, the film adhesive used in these applications is very effective at providing a good level of intrinsic adhesion such that the composite is found to fail rather than the film adhesive, as is typically the case in engineering applications.

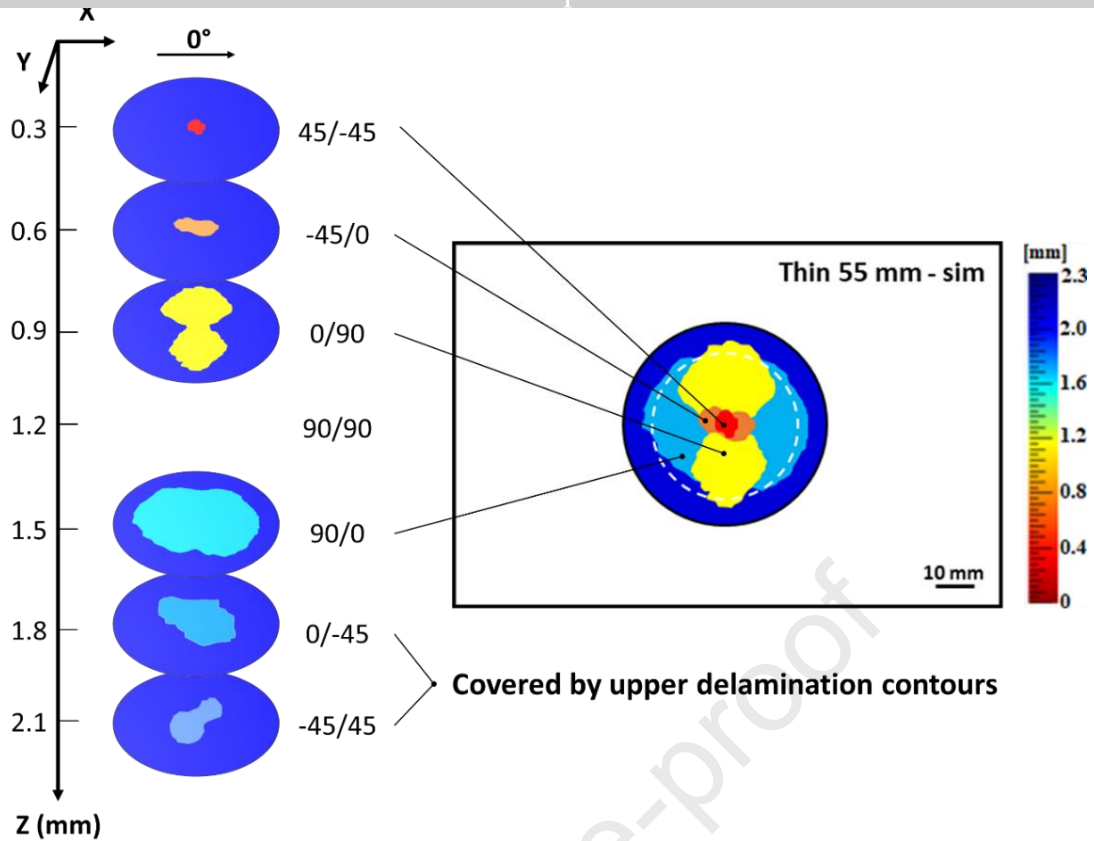


Fig. 12. An exploded view of the interlaminar damage at different interfaces in the multi-axial lay-up of the CFRP patch from the numerically-predictive simulations for the patch-repaired panel with a diameter of 55 mm and a thickness of 2.3 mm.

4.2.3. Intralaminar damage

Some of the post-impacted patch-repaired panels were examined using optical microscopy to study the formation of any intralaminar cracking in the patch. Fig. 13 shows two cross-sections comparing the experimentally-observed and numerically-predicted intralaminar matrix cracking damage in a patch from a post-impacted thin (i.e. 2.3 mm thickness) 55 mm diameter patch-repaired panel, where the red rectangle represents the region that has been inspected. There is relatively extensive intralaminar matrix cracking through the thickness of the patch. This has been accurately captured by the numerical model, which predicts a very similar distribution of intralaminar damage to the experimental observations. Interestingly, the cross-sectional damage map from the numerical simulation reveals a significant and continuous intralaminar matrix crack just above the central blocking 90° plies, which is in agreement with the optical micrograph. This was undoubtedly a precursor to the initiation and propagation of the major delaminations that occurred at the ply interfaces below and above the central-blocking 90° plies, as shown Fig. 12.

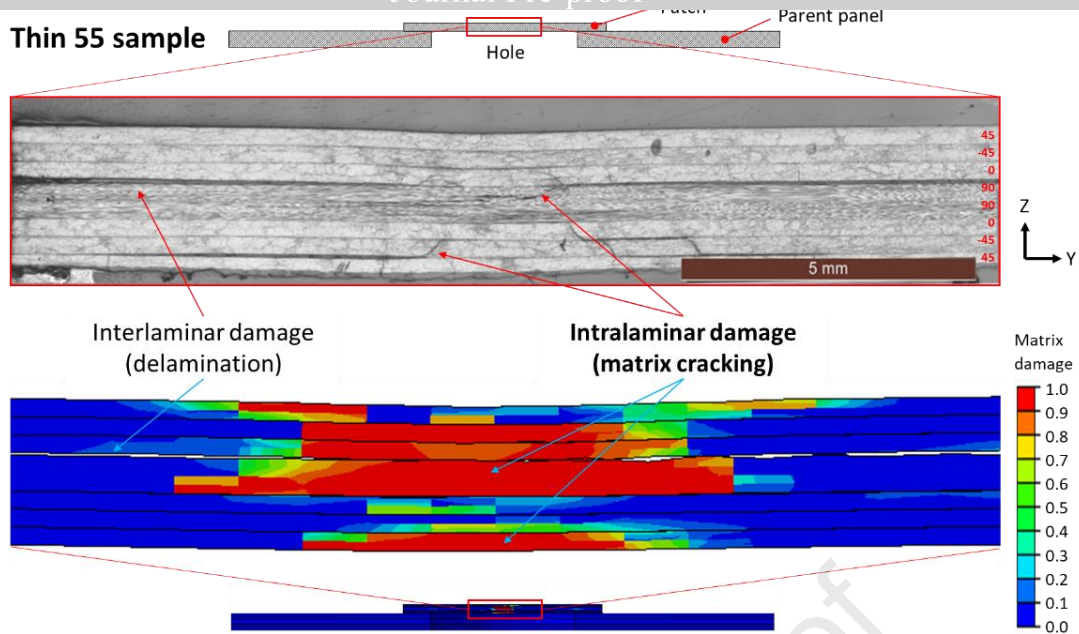


Fig. 13. Comparison between the experimentally-observed and numerically-predicted intralaminar matrix cracking damage in the thin (i.e. 2.3 mm thickness) 55 mm diameter patch-repaired panel.

4.2.4. Permanent indentation damage

Many experimental studies [30, 45, 48] have reported that a permanent indentation can be induced on the impacted surface of composite laminates when subjected to a low-velocity impact using a hard impactor. Fig. 14 presents the numerically-predicted indentation depths for the pristine and patch-repaired panels and Table 3 compares the predicted values with the experimentally-measured values. The predictions from the numerical model are in reasonable agreement with the experimental measurements. The thick (i.e. 4.6 mm thickness) 65 mm diameter patch-repaired panel exhibits the smallest depth of penetration for all the patch-repaired cases. The indentation consists of localised plastic deformation of the epoxy matrix and matrix cracking under the impactor site. Both of these processes are affected by the thickness of the patch and so variations in indentation depth and extent are observed. A problem for aircraft structures subject to impact is that the delamination damage is frequently hidden, or barely visible, and can often only be seen by C-scan inspection. This tell-tale indentation mark could therefore be a useful diagnostic tool.

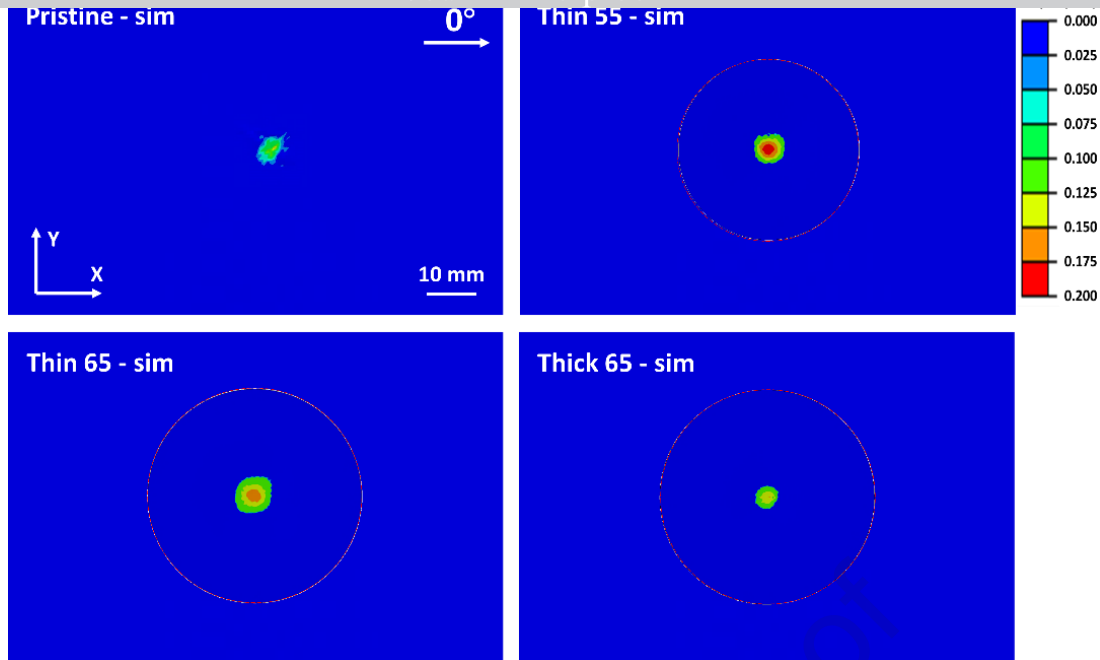


Fig. 14. Numerically predicted permanent indentation for the pristine and patch-repaired panels for different patch designs. (The scale on the right-hand side gives the indentation depth as a function of the colour used. The faint red circles indicate the diameter of the patch used, i.e. 55 mm or 65 mm.)

Table 3. Comparison between indentation depths obtained from experimental measurements and numerical predictions for the pristine and patch-repaired composite panels.

Design of panel	Pristine	Thin 55 mm	Thin 65 mm	Thick 65 mm
Measured depth (mm)	0.11 ± 0.02	0.16 ± 0.02	0.15 ± 0.02	0.12 ± 0.02
Predicted depth (mm)	0.128	0.193	0.172	0.135
Deviation	16.4%	20.6%	14.7%	18.2%

5. Results and discussion: comparisons between the non-plugged and plugged patch-repaired CFRP panels

5.1. Introduction

When repairing damaged composite laminates, the hole left after the damage has been cut-out is often filled, i.e. plugged, to further support the repair patch and to prevent fluids, e.g. water, fuel, etc., from accumulating in the empty space. Therefore, the effects of using a close-fitting plug on the impact behaviour of patch-repaired composites panels has been studied

5.2. Experimental results for impact loading responses and overall interlaminar damage

The load versus time and load versus displacement curves measured for the pristine panel and a patch-repaired panel using a thin (i.e. 2.3 mm thickness) patch with a 55 mm diameter are shown in Fig. 15, with values from these data also presented in Table 4. Again, the very good repeatability of the experimental data is noteworthy. The comparisons shown in Fig. 15 demonstrate that, when a plug is introduced, the bending stiffness of the patch-repaired composite panel significantly increased from about 2 kN/mm to about 5 kN/mm, which is also higher than the about 3 kN/mm of the pristine composite

panel. The duration time, maximum load and maximum displacement associated with the increase in the bending stiffness of the plugged panels also exhibit obvious changes compared to the pristine and non-plugged composite panels, as shown in Table 4. Based on these results it would appear that the presence of a plug in the hole, which replaces the cut-out damaged composite region, can benefit the repaired panel by increasing the stiffness and reducing the deformation due to external impact loading. However, a consequence of this is that there is a more abrupt load drop for the load response, from about 7.8 kN to just over 6 kN with accompanying oscillations in load, for the plugged composite panels. This load drop is believed to be caused by matrix cracking and subsequent delamination [49, 50]. The higher stiffness and higher maximum load, storing more strain energy, for the plugged composite panels, results in a more marked load drop, when compared with pristine and non-plugged composite panels.

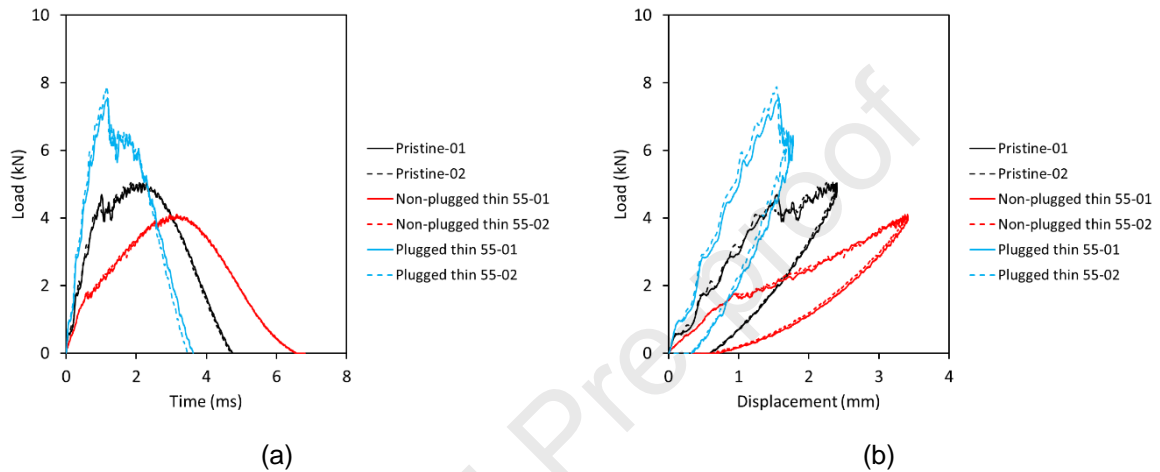


Fig. 15. Loading responses for the pristine and patch-repaired (plugged and non-plugged) composite panels for a thin (i.e. 2.3 mm thickness) 55 mm diameter patch: (a) the load versus time curves and (b) the load versus displacement curves.

Table 4. Comparison between the duration time of the impact event, maximum load and maximum displacement obtained for the pristine, plugged and non-plugged composite panels with a thin (i.e. 2.3 mm thickness) 55 mm diameter patch.

Design of panel:	Pristine	Non-plugged thin 55	Plugged thin 55
Duration time (ms)	$4.7 \pm 0.5\%$	$6.5 \pm 0.4\%$	$3.5 \pm 1.8\%$
Maximum load (kN)	$5.1 \pm 0.4\%$	$4.1 \pm 0.3\%$	$7.8 \pm 2.1\%$
Maximum displacement (mm)	$2.4 \pm 0.6\%$	$3.4 \pm 0.7\%$	$1.7 \pm 1.8\%$

Considering the overall delamination damage that was measured, the damage maps experimentally-measured from the C-scan inspection technique from the top and the bottom surfaces of the pristine and patch-repaired composite panels are presented in Fig. 16. (It should be noted that, due to the presence of the hole cut-out in the parent CFRP under the non-plugged repair patch, no C-scan maps could be obtained from the bottom surface inspection on the non-plugged panels.) A comparison of these damage maps shows that the plugged panel clearly exhibits the smallest damage footprint among these three panel designs. This confirms that the introduction of the CFRP plug significantly contributes to obtaining a very good impact performance of a patch-repaired composite panel, as shown in Fig. 15 and Table 4. The reason is that the presence of a plug increases the bending stiffness of the patch-

repaired composite panel and to decrease the out-of-plane displacement due to an impact load. As a result, this will constrain the growth of delaminations within the panel, which is reflected by the superior structural integrity of the plugged patch-repaired panel.

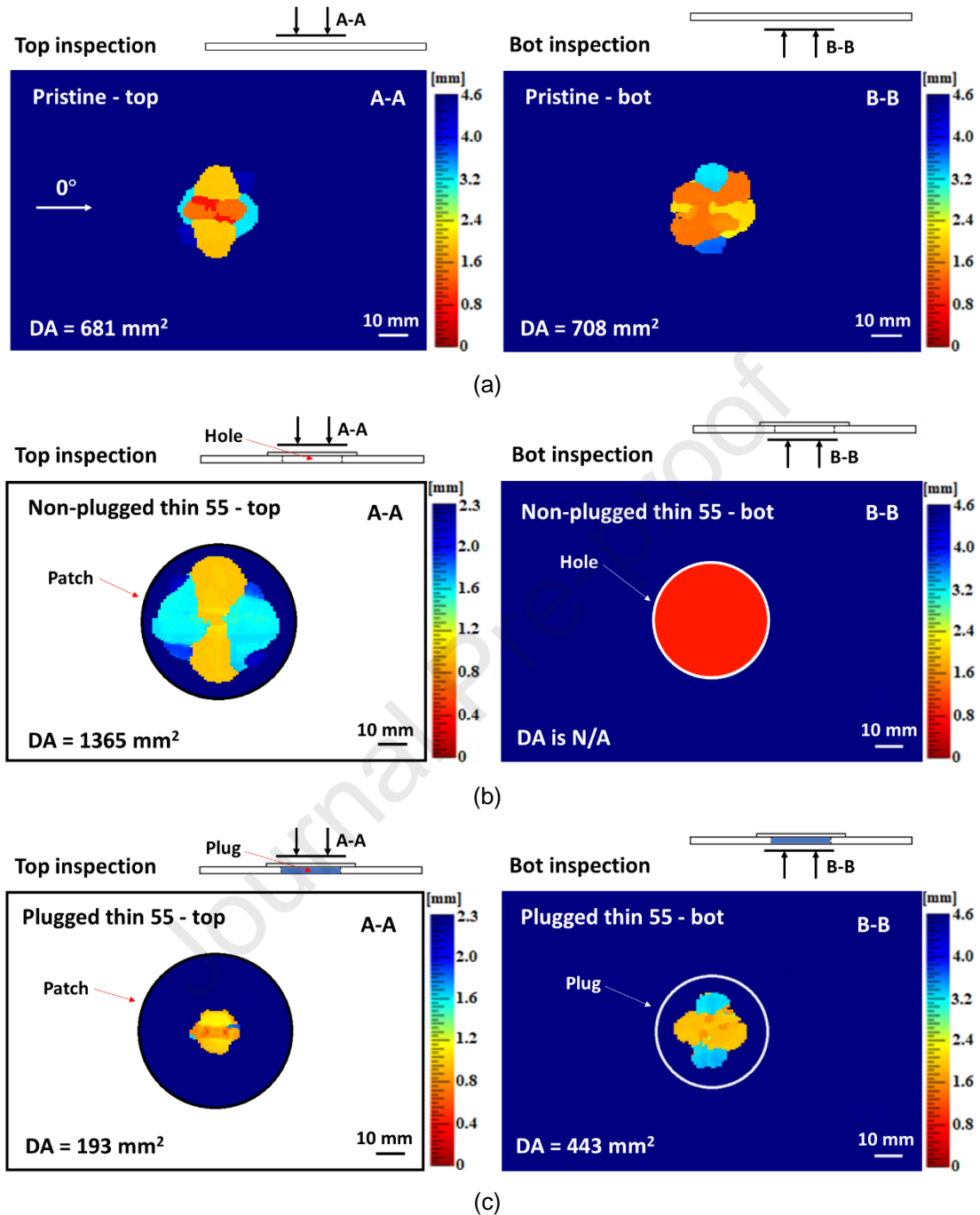


Fig. 16. Experimental (via C-scan inspection) damage footprints obtained for interlaminar, i.e. delamination, damage for the (a) pristine and (b) and (c) patch-repaired panels for thin (i.e. 2.3 mm thickness) 55 mm diameter patches: (b) without and (c) with CFRP plugs present. (Note that C-scan inspections have been conducted from both the top and bottom ('Bot') surfaces of the panels as indicated in the sketches.)

5.3.1. Overall loading response

Fig. 17 presents the loading responses obtained from experiment and numerical modelling simulations undertaken using the thin patch-repaired panels, with a 55 mm diameter patch and a plug. The experimentally-measured and numerically-predicted impact responses shown in Fig. 17 indicate that the numerical model can accurately capture the key features in the overall loading versus time curves, including the peak load and duration as well as the notable load drop, etc.

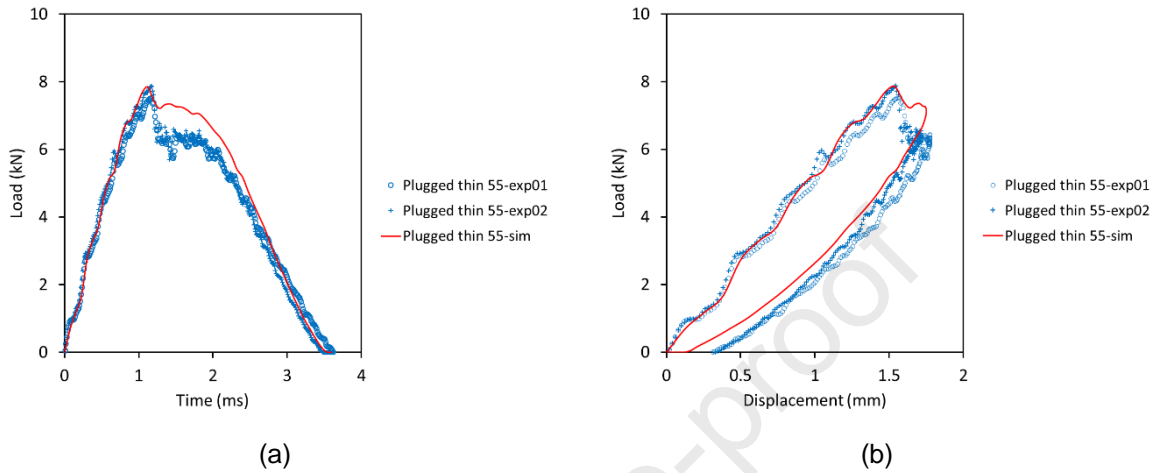


Fig. 17. Experimental and numerical loading responses obtained from the thin (i.e. thickness 2.3 mm) 55 mm diameter patch-repaired panels containing a plug: (a) Load versus time curves and (b) load versus displacement curves.

5.3.2. Interlaminar damage

Fig. 18 shows the experimentally-measured and numerically-predicted interlaminar damage footprint contours obtained from patch-repaired panels with thin (i.e. 2.3 mm thickness) 55 mm diameter patches with plugs as seen from (a) the top surface and (b) the bottom surface. The agreement between the experimental and numerical results is again good.

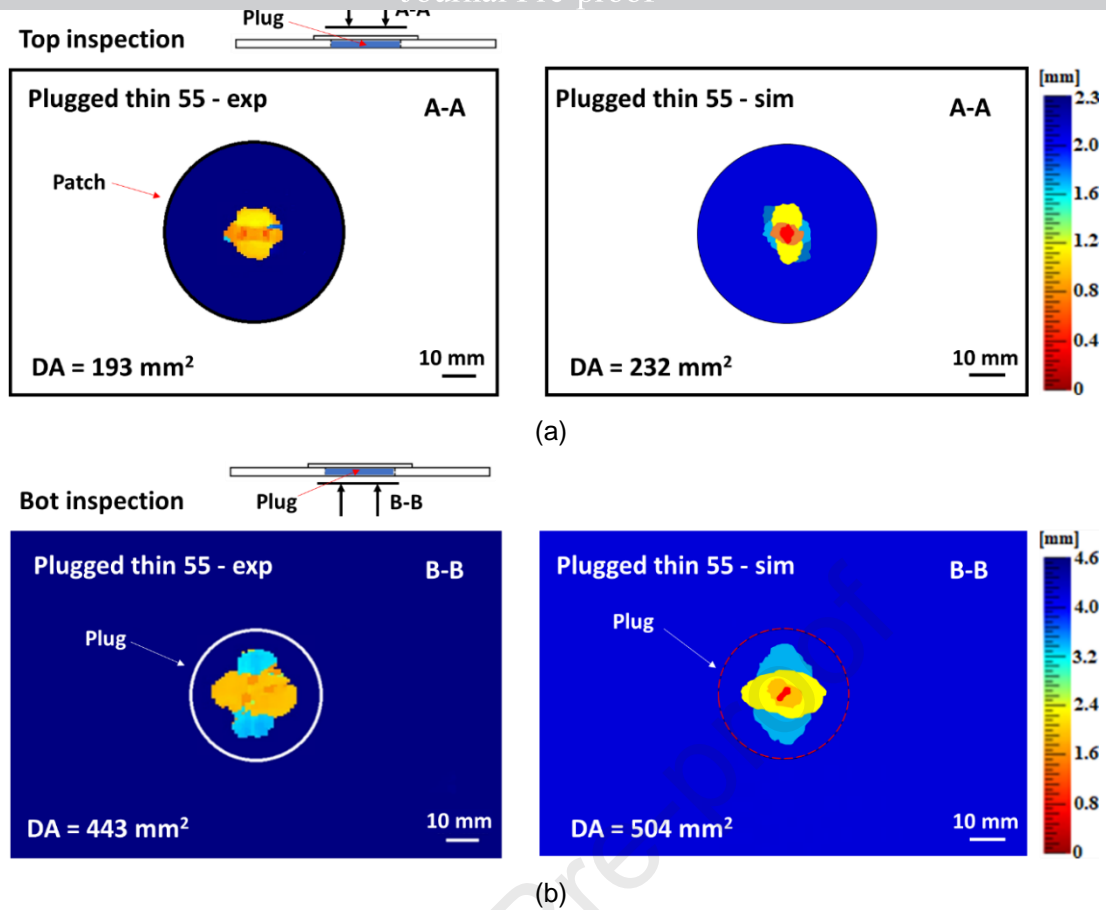


Fig. 18. Experimentally-measured and numerically-predicted damage footprint contours obtained from patch-repaired panels with thin (i.e. 2.3 mm thickness) 55 mm diameter patches with plugs as seen from (a) the top surface and (b) the bottom ('Bot') surface.

5.3.3. Intralaminar damage

Before considering a comparison between the experimentally-observed and numerically-predicted intralaminar damage in the thin (i.e. 2.3 mm thickness) 55 mm diameter patch-repaired panels with a CFRP plug, it is of interest to compare the experimental results for the thin (i.e. 2.3 mm thickness) 55 mm diameter patch-repaired panels with and without a plug present. Fig. 19 shows optical micrographs obtained from cross-sections of the (a) non-plugged and (b) the plugged thin (i.e. 2.3 mm thickness) 55 mm diameter patch-repaired panels, where the red rectangle represents the region that has been inspected. The micrographs of the non-plugged and plugged panels show that the interlaminar cracks, i.e. delaminations, at the interfaces near to the bottom surface were found to be linked with each other through 45° aligned intralaminar matrix cracks, which are formed due to the tensile stresses acting on the bottom plies. In the plugged panel, no detectable cracking is observed at the interfaces between the adhesive layer and the CFRP patch and the CFRP plug, as was indeed predicted from the modelling studies. However, obvious and continuous interlaminar cracking can be observed on the third interface (counting from top to bottom) which agrees with the C-scan results. The lengths of the interlaminar cracks in the patch-repaired panels containing a CFRP plug are considerably shorter than those seen in the non-plugged panels, which is reflected by the significantly smaller damage area in the C-scan maps, see Fig. 17. The good predictive capability of the proposed model is confirmed in Fig. 20, by

comparing the experimentally observed and numerically predicted intralaminar damage in the thin (i.e. 2.3 mm thickness) 55 mm diameter patch-repaired panels containing a plug.

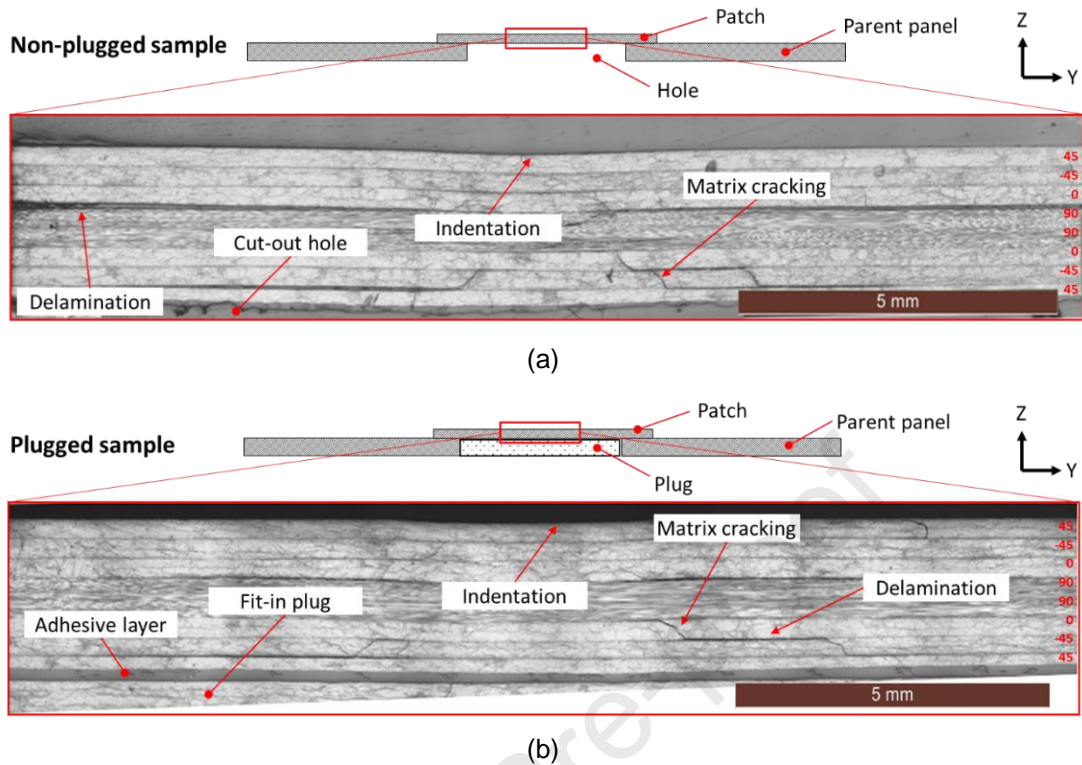


Fig. 19. Optical micrographs obtained from cross-sections of the (a) non-plugged and (b) the plugged thin (i.e. 2.3 mm thickness) 55 mm diameter patch-repaired panels.

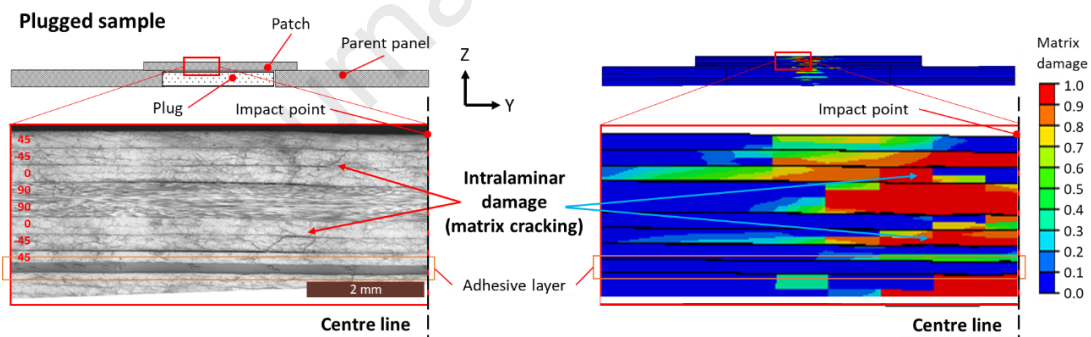


Fig. 20. Comparison between the experimentally-observed and numerically-predicted intralaminar damage in the thin (i.e. 2.3 mm thickness) 55 mm diameter patch-repaired panels with a CFRP plug.

5.3.4. Permanent indentation damage

Fig. 21 shows the indentation of the impacted surface of the thin (i.e. 2.3 mm thickness) 55 mm diameter patch-repaired panels containing a CFRP plug, for both: (a) the numerically-predicted indentation and (b) a comparison between the measured and predicted indentations. Fig. 21b shows that there is good agreement between the measured and predicted values of the permanent indentation. From Table 3 the measured permanent indentation of the corresponding non-plugged panel was $160 \pm 20 \mu\text{m}$, compared with $65 \pm 15 \mu\text{m}$ for the corresponding panel containing a plug. Thus, the plug significantly decreases the depth of permanent indentation that results from the impactor striking the patch. This

and the plug giving support to the repair and hence the plastic deformation in the patch is reduced, which leads to a reduction in the intralaminar and interlaminar damage by virtue of the presence of the supporting plug.

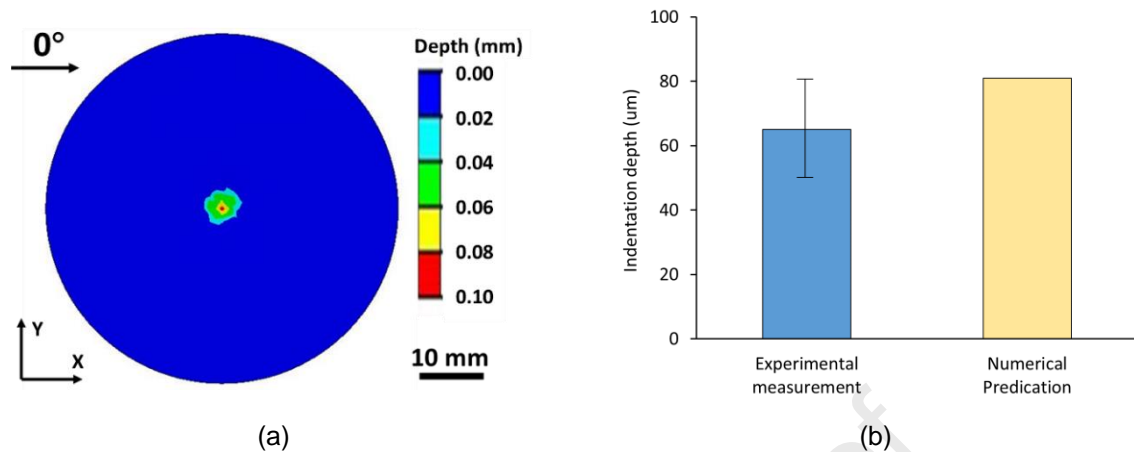


Fig. 21. Permanent indentation of the impacted surface of the thin (i.e. 2.3 mm thickness) 55 mm diameter patch-repaired panels containing a CFRP plug: (a) numerically-predicted indentation and (b) a comparison between the measured and predicted indentations.

5.3.5. Post-impact status of the adhesive layer

The damage maps of the adhesive layers in the non-plugged and plugged repaired panels were extracted from the numerical simulation and compared in Fig. 22. The comparison shows that minor damage in the adhesive layer was observed in the region near to the edge of the hole for the non-plugged repaired panel, whilst damage in the adhesive layer of the plugged repaired panel was only observed in the central area. Clearly, adding a plug alters the stress distribution in the repair structure. These results showed that the introduction of the plug can provide for protection of the adhesive bonding between the patch and the parent panel in the overlap region by providing more support. However, for the plugged case, some damage in the adhesive layer now occurs under the impact site.

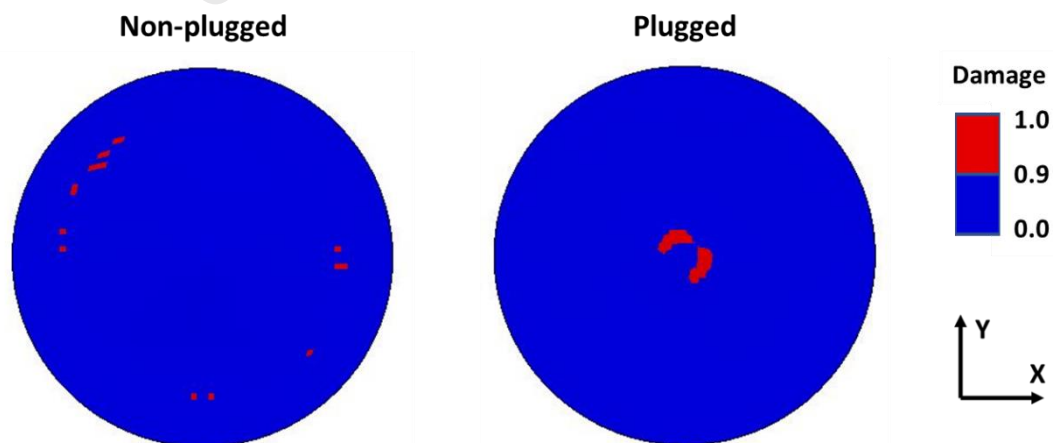


Fig. 22. Damage maps in the adhesive layer of patch-repaired panels for (a) non-plugged and (b) plugged cases, both with thin (i.e. 2.3 mm thickness) 55 mm diameter patches.

In this paper, the compressive strength and impact resistance of both the pristine and patch-repaired composite laminates are experimentally evaluated. Subsequently, a three-dimensional elastic-plastic computational model from [30] has been extended and employed to predict the impact behaviour of both pristine CFRP panels and various designs of patch-repaired CFRP panels. The key findings in this research are presented below:

- The 3-D FEA model is capable of replicating the load versus time and load versus displacement behaviour from drop-weight impact tests very well and accurately captures the damage initiation associated with load drops or changes in stiffness.
- Delaminations predicted using the 3-D FEA model exhibit a very similar shape and extent through the thickness of the panels as observed by C-scan inspection. Permanent indentations associated with the matrix plasticity and cracking are also accurately predicted.
- Comparison between the results of laminates repaired with different patches shows that a relatively thick patch can reduce the deformation and delamination of repaired laminates. However, an increase in the diameter of the patch has little effect once an adequate bonded-overlap is achieved.
- The presence of a plug in the hole, to replace the cut-out damaged region, can benefit the patch-repaired panel by increasing the stiffness of the patch-repaired region and so reducing the deformation and damage due to external impact loading.

In all cases, the 3-D FEA model is able to reasonably capture the overall deformation and damage of pristine and repaired composite laminates subjected to impact loading. Future research will focus on the effectiveness of different repair techniques for composite materials, so that the developed model can serve as a powerful design tool for composite repair.

Acknowledgements

The authors would like to thank Polar Manufacturing Ltd. for their assistance in manufacturing the patch-repaired CFRP composite panels. The impact damage model was presented at The Royal Society 'Griffith Centenary Virtual Conference on September 20-21, 2021' – an open access recording is available via The Royal Society website.

A.1 The intralaminar damage model for the CFRP laminates

A.1.1 The material response prior to the initiation of intralaminar damage

An extended elastic-plastic (E-P) constitutive model has been developed from previous research [30, 51, 52] to capture the material response prior to the initiation of matrix cracking and other failure processes and is given by:

$$\begin{Bmatrix} d\varepsilon_{11} \\ d\varepsilon_{22} \\ d\varepsilon_{33} \\ d\gamma_{12} \\ d\gamma_{13} \\ d\gamma_{23} \end{Bmatrix} = \begin{bmatrix} 1/E_{11} & -\nu_{21}/E_{11} & -\nu_{31}/E_{11} & 0 & 0 & 0 \\ -\nu_{12}/E_{22} & 1/E_{22} & -\nu_{32}/E_{22} & 0 & 0 & 0 \\ -\nu_{13}/E_{33} & -\nu_{23}/E_{33} & 1/E_{33} & 0 & 0 & 0 \\ 0 & 0 & 0 & 1/G_{12} & 0 & 0 \\ 0 & 0 & 0 & 0 & 1/G_{13} & 0 \\ 0 & 0 & 0 & 0 & 0 & 1/G_{23} \end{bmatrix} \begin{Bmatrix} d\sigma_{11} \\ d\sigma_{22} \\ d\sigma_{33} \\ d\tau_{12} \\ d\tau_{13} \\ d\tau_{23} \end{Bmatrix} + \begin{Bmatrix} d\varepsilon_{11}^p \\ d\varepsilon_{22}^p \\ d\varepsilon_{33}^p \\ d\gamma_{12}^p \\ d\gamma_{13}^p \\ d\gamma_{23}^p \end{Bmatrix} \quad (\text{A-1})$$

where $d\varepsilon_{ij}$ and $d\gamma_{ij}$ ($i, j = 1, 2, 3$) are the incremental total strains and $d\sigma_{ij}$ and $d\tau_{ij}$ ($i, j = 1, 2, 3$) are the incremental stresses. The terms ν_{ij} ($i, j = 1, 2, 3, i \neq j$) are the Poisson's ratios, E_{ii} ($i, j = 1, 2, 3, i = j$) are the Young's moduli either for tensile or compression loading, and G_{ij} ($i, j = 1, 2, 3, i \neq j$) are the shear moduli. The parameters $d\varepsilon_{ij}^p$ and $d\gamma_{ij}^p$ ($i, j = 1, 2, 3$) represent the incremental plastic strains, which are related to the equivalent stress, σ_{equ} , and the equivalent plastic strain, ε_{equ}^p . The equivalent stress, σ_{equ} , is given by:

$$\sigma_{equ} = \sqrt{\frac{3}{2}(\sigma_{22}^2 + \sigma_{33}^2) - 3\sigma_{22}\sigma_{33} + 3a_{44}\tau_{23}^2 + 3a_{55}\tau_{13}^2 + 3a_{66}\tau_{12}^2} \quad (\text{A-2})$$

where a_{44} , a_{55} and a_{66} are coefficients which indicate the extent of anisotropy in the plastic behaviour. For transversely isotropic solids which are linearly elastic in the fibre direction, i.e. a unidirectional fibre-reinforced composite, the value of the coefficient a_{44} , associated with the term τ_{23}^2 , can be set as having a value of two and the coefficient a_{55} , associated with τ_{13}^2 , is equal in value to the coefficient a_{66} , associated with τ_{12}^2 . Now, the coefficient a_{66} can be readily determined from off-axis tensile and compression experiments, relative to the fibre direction, using a unidirectional composite. The relationship between the effective stress, σ_{eff} , and the effective plastic strain, ε_{eff}^p , can be expressed as a power-law function, given by:

$$\varepsilon_{eff}^p = A\sigma_{eff}^n \quad (\text{A-3})$$

where A and n are the nonlinear coefficients, which can be determined by fitting to the σ_{eff} versus ε_{eff}^p data, again as obtained from the off-axis experiments are employed using a unidirectional composite e.g. [53-55]. Based on the determined single parameter, a_{66} , and the nonlinear coefficients, A and n , the incremental plastic strain tensors, $d\varepsilon_{ij}^p$ ($i, j = 1, 2, 3$), can be calculated as:

$$\begin{Bmatrix} d\varepsilon_{11}^p \\ d\varepsilon_{22}^p \\ d\varepsilon_{33}^p \\ d\gamma_{12}^p \\ d\gamma_{13}^p \\ d\gamma_{23}^p \end{Bmatrix} = \frac{An}{\sigma_{equ}^{1-n}} \begin{Bmatrix} 0 \\ 3(\sigma_{22} - \sigma_{33})/2\sigma_{equ} \\ 3(\sigma_{33} - \sigma_{22})/2\sigma_{equ} \\ 3a_{66}\tau_{12}/2\sigma_{equ} \\ 3a_{55}\tau_{13}/2\sigma_{equ} \\ 3a_{44}\tau_{23}/2\sigma_{equ} \end{Bmatrix} d\sigma_{equ} \quad (\text{A-4})$$

A.1.2 The initiation of intralaminar damage

The Northwestern University (NU) damage criteria were employed to capture the initiation of intralaminar damage in the CFRP laminates, such as matrix cracking, etc. The NU criteria were proposed by Daniel et al. [38, 56]. These 3-D criteria are partially interactive failure criteria, in which more than one stress component has been used to evaluate the different failure modes. The mathematical details of the damage initiation model for a composite ply are given in Table A-1, where σ_{ij} and τ_{ij} are the normal and shear stresses and F_{iT} ($i = 1,2,3$), F_{iC} ($i = 1,2,3$) and F_{iS} ($i = 2,3$) are the tensile, compressive and shear damage criteria in the three material directions, respectively, and the initiation of damage is predicted to occur when $F \geq 1$. The terms S_{it} ($i = 1,2,3$) are the tensile strengths in the three material directions and S_{ic} ($i = 1,2,3$) are the compressive strengths in the three material directions. Finally, S_{12} , S_{13} and S_{23} represent the shear strengths in the corresponding material directions. The use of these criteria for the initiation of intralaminar damage are included in the flow chart for the FEA model.

Table A-1

The mathematical definitions for the initiation of intralaminar damage.

Damage induced by	Criteria for damage initiation
Longitudinal tensile stresses	$F_{1T} = \left(\frac{\sigma_{11}}{S_{1t}}\right)^2 + \frac{\tau_{12}^2 + \tau_{13}^2}{S_{12}^2}$ for $\sigma_{11} \geq 0$ (A-5)
Longitudinal compressive stresses	$F_{1C} = \left(\frac{\sigma_{11}}{S_{1c}}\right)^2$ for $\sigma_{11} < 0$ (A-6)
Transverse tensile stresses	$F_{2T} = \frac{\sigma_{22}}{S_{2t}} + \left(\frac{E_{22}}{2G_{12}}\right)^2 \left(\frac{\tau_{12}}{S_{2t}}\right)^2 + \left(\frac{E_{22}}{2G_{23}}\right)^2 \left(\frac{\tau_{23}}{S_{2t}}\right)^2$ for $ \sigma_{22} \geq \tau_{12}(\tau_{23}) $ and $\sigma_{22} \geq 0$ (A-7)
Transverse compressive stresses	$F_{2C} = \left(\frac{\sigma_{22}}{S_{2c}}\right)^2 + \left(\frac{E_{22}}{G_{12}}\right)^2 \left(\frac{\tau_{12}}{S_{2c}}\right)^2 + \left(\frac{E_{22}}{G_{23}}\right)^2 \left(\frac{\tau_{23}}{S_{2c}}\right)^2$ for $ \sigma_{22} \geq \tau_{12}(\tau_{23}) $ and $\sigma_{22} < 0$ (A-8)
Transverse shear stresses	$F_{2S} = \left(\frac{\tau_{12}}{S_{12}}\right)^2 + \left(\frac{\tau_{23}}{S_{23}}\right)^2 + \frac{2G_{12}\sigma_{22}}{E_{22}S_{12}}$ for $ \sigma_{22} < \tau_{12}(\tau_{23}) $ (A-9)
Through-thickness tensile stresses	$F_{3T} = \frac{\sigma_{33}}{S_{3t}} + \left(\frac{E_{33}}{2G_{13}}\right)^2 \left(\frac{\tau_{13}}{S_{3t}}\right)^2 + \left(\frac{E_{33}}{2G_{23}}\right)^2 \left(\frac{\tau_{23}}{S_{3t}}\right)^2$ for $ \sigma_{33} \geq \tau_{13}(\tau_{23}) $ and $\sigma_{33} \geq 0$ (A-10)
Through-thickness compressive stresses	$F_{3C} = \left(\frac{\sigma_{33}}{S_{3c}}\right)^2 + \left(\frac{E_{33}}{G_{13}}\right)^2 \left(\frac{\tau_{13}}{S_{3c}}\right)^2 + \left(\frac{E_{33}}{G_{23}}\right)^2 \left(\frac{\tau_{23}}{S_{3c}}\right)^2$ for $ \sigma_{33} \geq \tau_{13}(\tau_{23}) $ and $\sigma_{33} < 0$ (A-11)
Through-thickness shear stresses	$F_{3S} = \left(\frac{\tau_{13}}{S_{13}}\right)^2 + \left(\frac{\tau_{23}}{S_{23}}\right)^2 + \frac{2G_{13}\sigma_{33}}{E_{33}S_{13}}$ for $ \sigma_{33} < \tau_{13}(\tau_{23}) $ (A-12)

The damage evolution law, based on the energy dissipated during the damage process and assuming linear material softening, was used to predict the evolution of the intralaminar damage in the composite skins. Corresponding to the damage initiation mechanisms defined in the NU damage criteria, eight damage parameters are defined in the damage evolution model. A general form of the damage variable for a particular damage initiation mechanism is given by [57]:

$$d = \frac{(\varepsilon^f - \varepsilon_p)(\varepsilon - \varepsilon^0)}{(\varepsilon - \varepsilon_p)(\varepsilon^f - \varepsilon^0)} \quad (\text{A-13})$$

where: when $d = d_{1t}$ this represents longitudinal tensile-dominated failure, when $d = d_{1c}$ this represents longitudinal compression-dominated failure, when $d = d_{2t}$ this represents transverse tensile-dominated failure, when $d = d_{2c}$ this represents transverse compression-dominated failure and when $d = d_{2s}$ this refers to transverse shear-dominated failure. Similarly, when $d = d_{3t}$ this represents through-thickness tensile-dominated failure, and when $d = d_{3c}$ and $d = d_{3s}$ these refer to the through-thickness compression-dominated failure and through-thickness shear-dominated failure, respectively. The strains, ε and ε_p , are the combined total strain and the combined plastic strain respectively in the composite ply. The strain values, ε^0 and ε^f , are the combined strains corresponding to initial failure and final failure, respectively. For longitudinal tension or compression failure, the strains ε , ε^0 and ε^f would be assigned to be $\varepsilon = \varepsilon_{11}$, $\varepsilon^0 = \varepsilon_{11}^0$ and $\varepsilon^f = \varepsilon_{11}^f$, respectively. For transverse tension or compression failure, the strains ε , ε^0 and ε^f would be assigned to be $\varepsilon = \sqrt{\varepsilon_{22}^2 + \gamma_{12}^2 + \gamma_{23}^2}$, $\varepsilon^0 = \sqrt{\varepsilon_{22}^0{}^2 + \gamma_{12}^0{}^2 + \gamma_{23}^0{}^2}$ and $\varepsilon^f = \sqrt{\varepsilon_{22}^f{}^2 + \gamma_{12}^f{}^2 + \gamma_{23}^f{}^2}$, respectively, noting that $\gamma_{ij} = 2 \varepsilon_{ij}$. For through-thickness tension or compression failure, the strains ε , ε^0 and ε^f would be assigned to be $\varepsilon = \sqrt{\varepsilon_{33}^2 + \gamma_{23}^2 + \gamma_{13}^2}$, $\varepsilon^0 = \sqrt{\varepsilon_{33}^0{}^2 + \gamma_{23}^0{}^2 + \gamma_{13}^0{}^2}$ and $\varepsilon^f = \sqrt{\varepsilon_{33}^f{}^2 + \gamma_{23}^f{}^2 + \gamma_{13}^f{}^2}$, respectively. The final failure strain, ε_{ij}^f ($i, j = 1, 2, 3$), can be determined through the following equation [13, 58]:

$$\varepsilon_{ij}^f = 2G_{ij}/(\sigma_{ij}^0 l_c) \quad (\text{A-14})$$

where the respective values of $G_c|_{ij}$ are the tensile, $G_{1c}|_{ft}$, and compressive, $G_{1c}|_{fc}$, intralaminar ply fracture energies in the longitudinal fibre-direction, and for the transverse direction are the tensile, $G_{1c}|_{mt}$, compressive, $G_{1c}|_{mc}$, and shear, $G_{11c}|_{ms}$, intralaminar ply fracture energies. The term σ_{ij}^0 is the stress corresponding to damage initiation and l_c is the characteristic length which can be determined based on the volume of the elements.

A.2 The interlaminar damage model for the CFRP laminates

A.2.1 Initiation of interlaminar damage

Interlaminar damage typically involves the initiation and growth of delaminations, i.e. interlaminar cracking, between the plies that make up the composite skins and this was captured using the 'Abaqus/Explicit' built-in cohesive law (i.e. interface) element, having a zero thickness, using a fracture-mechanics approach. The interface element was described via a cohesive (i.e. damage) surface law [59-63] where a traction, t , is a function of the displacement, δ , and is in the form of a bilinear cohesive

law for a linear-elastic material model with a stiffness, k_i , and an initial stiffness of the interface elements were inserted between each ply of composite material in the CFRP laminates, using the properties shown in Table 1 for the CFRP. For the interlaminar failure, a quadratic-traction criterion was employed to capture the damage initiation in the interface, as given by [64]:

$$\left(\frac{\langle t_{33} \rangle}{t_{33}^0}\right)^2 + \left(\frac{t_{31}}{t_{31}^0}\right)^2 + \left(\frac{t_{32}}{t_{32}^0}\right)^2 = 1 \quad (\text{A-15})$$

where t_i ($i = 33, 31, 32$) represent the current normal and shear tractions and t_i^0 ($i = 33, 31, 32$) represent the normal and shear cohesive strengths. The corresponding displacements are denoted by δ_{33} , δ_{31} and δ_{32} , and by δ_{33}^0 , δ_{31}^0 and δ_{32}^0 , respectively. The value of the cohesive strength, t_{33}^0 , was determined from the theory proposed in [65, 66], which maintains computation accuracy whilst avoiding a very fine mesh and a commensurate increase in computational cost, and for the shear cohesive strengths then $t_{31}^0 = t_{32}^0$. Thus, the onset of damage initiation at δ^0 which may be defined at a value of the combined displacement in the cohesive law when:

$$\sqrt{\langle \delta_{33}^2 \rangle + \delta_{31}^2 + \delta_{32}^2} = \sqrt{\langle \delta_{33}^{0^2} \rangle + \delta_{31}^{0^2} + \delta_{32}^{0^2}} \quad (\text{A-16})$$

A.2.2 Evolution of interlaminar damage

The energy-based Benzeggagh-Kenane (B-K) [67, 68] criterion for Mixed-mode propagation was used to derive a total value G_c for the growth of the delamination and is given by:

$$G_c = G_{Ic} + (G_{IIc} - G_{Ic}) \left(\frac{G_I + G_{III}}{G_I + G_{II} + G_{III}} \right)^\eta \quad (\text{A-17})$$

where G_{Ic} is the Mode I (opening tensile), G_{IIc} is the Mode II (in-plane shear) interlaminar fracture energy, and η is the B-K Mixed-mode interaction exponent. The values of G_{Ic} , G_{IIc} and η may all be experimentally measured [69, 70] and so inputted into the FEA model. The parameters G_I , G_{II} and G_{III} are the current Mode I (opening tensile), Mode II (in-plane shear) and Mode III (anti-plane shear) energy-release rates, respectively, as calculated from the FEA code. For the node at the interlaminar crack tip, an interlaminar damage parameter, d_{inter} , may be defined from degrading the initial cohesive stiffness, k_i ($i = 33, 31, 32$) as the interlaminar damage after initiation, when $\delta = \delta^0$, now evolves to the point when separation, i.e. interlaminar cracking, occurs at $\delta = \delta^f$. Now, this interlaminar damage parameter, d_{inter} , starts with a value of 0 when $\delta = \delta^0$ and finishes with a value of 1 when $\delta = \delta^f$ according to the relationship:

$$d_{inter} = \frac{\delta^f (\delta - \delta^0)}{\delta (\delta^f - \delta^0)} \quad (\text{A-18})$$

where the term $\delta = \sqrt{\langle \delta_{33}^2 \rangle + \delta_{31}^2 + \delta_{32}^2}$ is the combined displacement at a delamination interface.

The onset of damage initiation at δ^0 occurs when $\sqrt{\langle \delta_{33}^2 \rangle + \delta_{31}^2 + \delta_{32}^2} = \sqrt{\langle \delta_{33}^{0^2} \rangle + \delta_{31}^{0^2} + \delta_{32}^{0^2}}$, and failure of the interface element occurs, at δ^f when $\sqrt{\langle \delta_{33}^2 \rangle + \delta_{31}^2 + \delta_{32}^2} = \sqrt{\langle \delta_{33}^{f^2} \rangle + \delta_{31}^{f^2} + \delta_{32}^{f^2}}$. Here

the terms u_{33} , v_{31} and w_{32} are the displacements, corresponding to the stresses σ_{33} , τ_{31} and τ_{32} , in the cohesive law after damage has been initiated.

References

- [1] W. Cantwell and J. Morton, Detection of impact damage in CFRP laminates, *Compos. Struct.* 3 (1985) 241-257.
- [2] G. Dorey, S. Bishop and P. Curtis, On the impact performance of carbon fibre laminates with epoxy and PEEK matrices, *Compos. Sci. Technol.* 23 (1985) 221-237.
- [3] W. Cantwell and J. Morton, Comparison of the low and high velocity impact response of CFRP, *Composites* 20 (1989) 545-551.
- [4] W. Cantwell and J. Morton, The influence of varying projectile mass on the impact response of CFRP, *Compos. Struct.* 13 (1989) 101-114.
- [5] M.G. Nejhad and A. Parvizi-Majidi, Impact behaviour and damage tolerance of woven carbon fibre-reinforced thermoplastic composites, *Composites* 21 (1990) 155-168.
- [6] W.J. Cantwell and J. Morton, The impact resistance of composite materials—a review, *composites* 22 (1991) 347-362.
- [7] H. Morita, T. Adachi, Y. Tateishi and H. Matsumot, Characterization of impact damage resistance of CF/PEEK and CF/toughened epoxy laminates under low and high velocity impact tests, *J. Reinf. Plast. Compos.* 16 (1997) 131-143.
- [8] R. Batra, G. Gopinath and J. Zheng, Damage and failure in low energy impact of fiber-reinforced polymeric composite laminates, *Compos. Struct.* 94 (2012) 540-547.
- [9] Y. Shi, T. Swait and C. Soutis, Modelling damage evolution in composite laminates subjected to low velocity impact, *Compos. Struct.* 94 (2012) 2902-2913.
- [10] Y. Shi, C. Pinna and C. Soutis, Modelling impact damage in composite laminates: a simulation of intra-and inter-laminar cracking, *Compos. Struct.* 114 (2014) 10-19.
- [11] H. Liu, B.G. Falzon and W. Tan, Experimental and numerical studies on the impact response of damage-tolerant hybrid unidirectional/woven carbon-fibre reinforced composite laminates, *Composites Part B: Engineering* 136 (2018) 101-118.
- [12] H. Liu, J. Liu, Y. Ding, J. Zheng, X. Kong, J. Zhou, L. Harper, B.R. Blackman, A.J. Kinloch and J.P. Dear, The behaviour of thermoplastic and thermoset carbon fibre composites subjected to low-velocity and high-velocity impact, *Journal of Materials Science* 55 (2020) 15741-15768.
- [13] H. Liu, J. Liu, Y. Ding, J. Zhou, X. Kong, B.R. Blackman, A.J. Kinloch, B.G. Falzon and J.P. Dear, Effects of impactor geometry on the low-velocity impact behaviour of fibre-reinforced composites: an experimental and theoretical investigation, *Appl. Compos. Mater.* 27 (2020) 533-553.
- [14] EDF renewables Wind Turbine Blade optimization and Efficiency Solutions Brochure at (2019): <https://www.edf-re.com/wp-content/uploads/Blade-Services-brochure-2019-FINAL-digital.pdf>
- [15] A.A. Baker, L.F. Rose and R. Jones, *Advances in the bonded composite repair of metallic aircraft structure*, Elsevier (2003).
- [16] C.H. Wang and C.N. Duong, *Bonded joints and repairs to composite airframe structures*, Academic Press (2015).
- [17] A. Rider, C. Wang and P. Chang, Bonded repairs for carbon/BMI composite at high operating temperatures, *Composites Part A: Applied Science and Manufacturing* 41 (2010) 902-912.
- [18] K.B. Katnam, L. Da Silva and T. Young, Bonded repair of composite aircraft structures: A review of scientific challenges and opportunities, *Progress in Aerospace Sciences* 61 (2013) 26-42.
- [19] C. Soutis, D. Duan and P. Goutas, Compressive behaviour of CFRP laminates repaired with adhesively bonded external patches, *Compos. Struct.* 45 (1999) 289-301.
- [20] F. Hu and C. Soutis, Strength prediction of patch-repaired CFRP laminates loaded in compression, *Compos. Sci. Technol.* 60 (2000) 1103-1114.

- fibre reinforced polymer panels, *Materials & Design* (1980-2015) 54 (2014) 174-183.
- [22] S. Coelho, P. Reis, J. Ferreira and A. Pereira, Effects of external patch configuration on repaired composite laminates subjected to multi-impacts, *Compos. Struct.* 168 (2017) 259-265.
- [23] Y. Tie, Y. Hou, C. Li, X. Zhou, T. Sapanathan and M. Rachik, An insight into the low-velocity impact behavior of patch-repaired CFRP laminates using numerical and experimental approaches, *Compos. Struct.* 190 (2018) 179-188.
- [24] Y. Hou, Y. Tie, C. Li, T. Sapanathan and M. Rachik, Low-velocity impact behaviors of repaired CFRP laminates: Effect of impact location and external patch configurations, *Composites Part B: Engineering* 163 (2019) 669-680.
- [25] T. Ouyang, W. Sun, R. Bao and R. Tan, Effects of matrix cracks on delamination of composite laminates subjected to low-velocity impact, *Compos. Struct.* 262 (2021) 113354.
- [26] M. Rezasefat, A. Gonzalez-Jimenez, M. Giglio and A. Manes, Numerical study on the dynamic progressive failure due to low-velocity repeated impacts in thin CFRP laminated composite plates, *Thin Wall Struct.* 167 (2021) 108220.
- [27] M. McElroy, A. André, T. Goode, S. Costa, R. Olsson and M. Pankow, Use of enriched shell elements compared to solid elements for modelling delamination growth during impact on composites, *Compos. Struct.* 269 (2021) 113945.
- [28] A. Katunin, A. Wronkiewicz-Katunin, W. Danek and M. Wyleżół, Modeling of a realistic barely visible impact damage in composite structures based on NDT techniques and numerical simulations, *Compos. Struct.* 267 (2021) 113889.
- [29] O. Falcó, C. Lopes, D. Sommer, D. Thomson, R. Ávila and B. Tijs, Experimental analysis and simulation of low-velocity impact damage of composite laminates, *Compos. Struct.* 287 (2022) 115278.
- [30] H. Liu, J. Liu, Y. Ding, Z.E. Hall, X. Kong, J. Zhou, B.R. Blackman, A.J. Kinloch and J.P. Dear, A three-dimensional elastic-plastic damage model for predicting the impact behaviour of fibre-reinforced polymer-matrix composites, *Composites Part B: Engineering* 201 (2020) 108389.
- [31] ASTM D7136/D7136M-14, Standard test method for measuring the damage resistance of a fiber-reinforced polymer matrix composite to a drop-weight impact event, West Conshohocken, PA.
- [32] T. Torrado, Experimental analysis and numerical optimisation of the effect of trigger mechanism on the energy absorption capabilities of composite tubular structures under impact loading, School of Aerospace, Transport and Manufacturing, Cranfield University, UK, 2018.
- [33] A. Ramji, Y. Xu, M. Yasaei, M. Grasso and P. Webb, Delamination migration in CFRP laminates under mode I loading, *Compos. Sci. Technol.* 190 (2020) 108067.
- [34] A. Ramji, Y. Xu, M. Yasaei, M. Grasso and P. Webb, Influence of veil interleave distribution on the delamination resistance of cross-ply CFRP laminates under low velocity impact, *Int. J. Impact Eng.* 157 (2021) 103997.
- [35] M. Abir, T. Tay, M. Ridha and H. Lee, On the relationship between failure mechanism and compression after impact (CAI) strength in composites, *Compos. Struct.* 182 (2017) 242-250.
- [36] C. Liljedahl, A. Crocombe, M. Wahab and I. Ashcroft, Modelling the environmental degradation of adhesively bonded aluminium and composite joints using a CZM approach, *Int. J. Adhes. Adhes.* 27 (2007) 505-518.
- [37] B. Blackman, J. Dear, A. Kinloch, H. Macgillivray, Y. Wang, J. Williams and P. Yayla, The failure of fibre composites and adhesively bonded fibre composites under high rates of test, *Journal of Materials Science* 30 (1995) 5885-5900.
- [38] I.M. Daniel, J.-J. Luo and P.M. Schubel, Three-dimensional characterization of textile composites, *Composites Part B: Engineering* 39 (2008) 13-19.
- [39] I.M. Daniel, J.-J. Luo, P.M. Schubel and B.T. Werner, Interfiber/interlaminar failure of composites under multi-axial states of stress, *Compos. Sci. Technol.* 69 (2009) 764-771.
- [40] I.M. Daniel, Failure of composite materials, *Strain* 43 (2007) 4-12.

materials science 26 (1991) 2124-2132.

[42] B. Crouch and J. Williams, Modelling of dynamic crack propagation behaviour in the three-point bend impact specimen, *J. Mech. Phys. Solids* 36 (1988) 1-13.

[43] J. Williams and G. Adams, The analysis of instrumented impact tests using a mass-spring model, *International Journal of Fracture* 33 (1987) 209-222.

[44] J. Dear, High-speed photography of impact effects in three-point bend testing of polymers, *J. Appl. Phys.* 67 (1990) 4304-4312.

[45] J. Bienias, P. Jakubczak and B. Surowska, Comparison of polymer composites behavior to low-velocity impact and quasi-static indentation, *Composites Theory and Practice* 13 (2013) 155-159.

[46] Z. Hall, J. Liu, R. Brooks, H. Liu, J. Crocker, A. Joesbury, L. Harper, B. Blackman, A. Kinloch and J. Dear, The effectiveness of patch repairs to restore the impact properties of carbon-fibre reinforced-plastic composites, *Engineering Fracture Mechanics* (2022) 108570.

[47] H. Liu, R. Brooks, Z. Hall, J. Liu, J. Crocker, A. Joesbury, L. Harper, B. Blackman, A. Kinloch and J. Dear, Experimental and numerical investigations on the impact behaviour of pristine and patch-repaired composite laminates, *Philosophical Transactions of the Royal Society A* 380 (2022) 20210340.

[48] C. Bouvet, S. Rivallant and J.-J. Barrau, Low velocity impact modeling in composite laminates capturing permanent indentation, *Compos. Sci. Technol.* 72 (2012) 1977-1988.

[49] H. Kaczmarek and S. Maison, Comparative ultrasonic analysis of damage in CFRP under static indentation and low-velocity impact, *Compos. Sci. Technol.* 51 (1994) 11-26.

[50] G. Davies and R. Olsson, Impact on composite structures, *The Aeronautical Journal* 108 (2004) 541-563.

[51] C. Weeks and C. Sun, Modeling non-linear rate-dependent behavior in fiber-reinforced composites, *Compos. Sci. Technol.* 58 (1998) 603-611.

[52] C. Sun and J. Chen, A simple flow rule for characterizing nonlinear behavior of fiber composites, *J. Compos. Mater.* 23 (1989) 1009-1020.

[53] J. Chen, F. Allahdadi and C. Sun, A quadratic yield function for fiber-reinforced composites, *J. Compos. Mater.* 31 (1997) 788-811.

[54] T. Yokozeki, S. Ogiwara, S. Yoshida and T. Ogasawara, Simple constitutive model for nonlinear response of fiber-reinforced composites with loading-directional dependence, *Compos. Sci. Technol.* 67 (2007) 111-118.

[55] K. Yoon and C. Sun, Characterization of elastic-viscoplastic properties of an AS4/PEEK thermoplastic composite, *J. Compos. Mater.* 25 (1991) 1277-1296.

[56] I. Daniel, B. Werner and J. Fenner, Strain-rate-dependent failure criteria for composites, *Compos. Sci. Technol.* 71 (2011) 357-364.

[57] D. Systèmes, Abaqus 2018 Documentation, Providence, USA (2017).

[58] H. Liu, B.G. Falzon, S. Li, W. Tan, J. Liu, H. Chai, B.R. Blackman and J.P. Dear, Compressive failure of woven fabric reinforced thermoplastic composites with an open-hole: an experimental and numerical study, *Compos. Struct.* 213 (2019) 108-117.

[59] R.D.S.G. Campilho, M. De Moura, A. Pinto, J. Morais and J. Domingues, Modelling the tensile fracture behaviour of CFRP scarf repairs, *Composites Part B: Engineering* 40 (2009) 149-157.

[60] R.D. Campilho, M. De Moura and J. Domingues, Using a cohesive damage model to predict the tensile behaviour of CFRP single-strap repairs, *International Journal of Solids and Structures* 45 (2008) 1497-1512.

[61] D.S. Dugdale, Yielding of steel sheets containing slits, *J. Mech. Phys. Solids* 8 (1960) 100-104.

[62] G.I. Barenblatt, The mathematical theory of equilibrium cracks in brittle fracture, *Adv. Appl. Mech.* 7 (1962) 55-129.

[63] Y. Shi, C. Pinna and C. Soutis, Interface cohesive elements to model matrix crack evolution in composite laminates, *Appl. Compos. Mater.* 21 (2014) 57-70.

(1988) 1141-1155.

[65] A. Turon, C.G. Dávila, P.P. Camanho and J. Costa, An engineering solution for mesh size effects in the simulation of delamination using cohesive zone models, *Engineering Fracture Mechanics* 74 (2007) 1665-1682.

[66] A. Turon, P.P. Camanho, J. Costa and J. Renart, Accurate simulation of delamination growth under mixed-mode loading using cohesive elements: Definition of interlaminar strengths and elastic stiffness, *Compos. Struct.* 92 (2010) 1857-1864.

[67] P.P. Camanho, C.G. Davila and M.F. de Moura, Numerical Simulation of Mixed-Mode Progressive Delamination in Composite Materials, *J. Compos. Mater.* 37 (2003) 1415-1438.

[68] M.L. Benzeggagh and M. Kenane, Measurement of mixed-mode delamination fracture toughness of unidirectional glass/epoxy composites with mixed-mode bending apparatus, *Compos. Sci. Technol.* 56 (1996) 439-449.

[69] C. Sarrado, A. Turon, J. Renart and I. Urresti, Assessment of energy dissipation during mixed-mode delamination growth using cohesive zone models, *Composites Part A: Applied Science and Manufacturing* 43 (2012) 2128-2136.

[70] S. Hashemi, A.J. Kinloch and J. Williams, The analysis of interlaminar fracture in uniaxial fibre-polymer composites, *Proceedings of the Royal Society of London. A. Mathematical and Physical Sciences* 427 (1990) 173-199.

Highlights:

- Pristine CFRP panels and Single-sided CFRP patch-repaired panels with and without plugs are prepared and impacted at an energy of 7.5 J;
- Effects of the diameter and thickness of the patch as well as the presence of plug on the impacted behaviour of repaired composites are investigated;
- Good correlation, between the experiment and simulation demonstrates that the developed numerical model is a useful design tool;
- The results revealed that the patch thickness has larger effects on the impact behaviour of repaired composites compared to the patch diameter;
- A plug can provide added structural integrity to a composite repair and reduce damage in the adhesive bond.

Declaration of interests

The authors declare that they have no known competing financial interests or personal relationships that could have appeared to influence the work reported in this paper.

The authors declare the following financial interests/personal relationships which may be considered as potential competing interests:

Journal Pre-proof